APPLICATIONS OF ALGINATE HYDROGELS AND POROUS SILICON IN DRUG DELIVERY AND TISSUE ENGINEERING

by

Alexa Frattini

Submitted in partial fulfillment of the
requirements for Departmental Honors in
the Department of Chemistry and Biochemistry
Texas Christian University
Fort Worth, Texas

May 2, 2022

APPLICATIONS OF ALGINATE HYDROGELS AND POROUS SILICON IN DRUG DELIVERY AND TISSUE ENGINEERING

Project Approved:

Supervising Professor: Jeff Coffer, Ph.D.

Department of Chemistry and Biochemistry

Kayla Green, Ph.D.

Department of Chemistry and Biochemistry

Giridhar Akkaraju, Ph.D.

Department of Biology

ABSTRACT

Tissue engineering encompasses many important medical applications that pertain to the repair and regeneration of various tissues throughout the human body that have been adversely affected by disease or injury. Through combining the body's cells with synthetic scaffolds, tissue engineering promotes proliferation of cells at damaged sites. Recent advances have demonstrated that using biocompatible materials such as alginate hydrogels—polymer networks derived from brown algae—are a cheap and environmentally-friendly approach to this. Alginate hydrogels are effective because they mimic the extracellular matrix of tissues, which provides structural support to cells that comprise human tissues.

One necessary modification to these scaffold materials is to load them with drugs that can facilitate healing. More complex designs can ideally deliver more than one therapeutic species simultaneously. In addition to hydrogels, drugs can also be loaded into a material known as porous silicon (pSi). pSi nanoparticles can be physically entrapped inside alginate hydrogels to create a two-system drug delivery mechanism with sustained release. This allows drugs such as growth factors, substances that stimulate cell growth, to be released at different times as the pSi and alginate hydrogel degrade with different timescales.

This project entails the construction of alginate hydrogels that incorporate model dye-loaded pSi particles. The release of two dye molecules known as curcumin and rhodamine were monitored to assess the efficacy of the two-system drug delivery process. It was first found that curcumin was too hydrophobic to achieve significant loading in the pSi. Rhodamine (R6G) was found to be released from the pSi/alginate hydrogel system in a more incremental (sustained) manner over time compared to a relatively large initial 'burst' release observed for the release of R6G from pSi only. Sustained release in drug delivery is important to ideally reduce the amount

of drug necessary and is in contrast to a burst release where large amounts of the loaded molecules are released prior to achieving a stable release profile. Furthermore, the localization of pSi in the alginate hydrogels was achieved by inserting R6G-loaded pSi membranes into pre-gelled alginate hydrogels, which is important to control the spatial delivery of the loaded molecule from pSi. Overall, it is believed that in the long term this pSi/alginate hydrogel material can greatly benefit the field of tissue engineering by creating dual delivery platforms with more diverse control over drug release.

Acknowledgements

This thesis project was made possible through the Texas Christian University Department of Chemistry and Biochemistry, as well as the Science and Engineering Research Center grant.

I would like to thank my research supervisor, Dr. Jeff Coffer, for supporting and guiding me throughout this process of inquiry and discovery. He always provided meaningful ideas and feedback both in the lab and at group meetings. I will forever be thankful for his constant encouragement and support throughout my undergraduate academic career.

Furthermore, I would like to thank the graduate students from Dr. Coffer's lab. First, Will always made himself available to answer questions, taught me how to use the instrumentation in the lab, and provided ideas to help me problem solve. Nguyen also assisted me whenever I needed it throughout my first semester in the lab. Additionally, Maegyn and Leo were always there to lend a helping hand in the lab and give meaningful feedback during group meetings.

I would also like to thank Youanna, my fellow lab partner and friend, for always keeping me company while working in the lab—there was truly never a dull moment when she was around.

Finally, I would like to thank my family, especially my parents, for always supporting me throughout my life. Without them, I would not be where I am today. My family and friends always challenged me to go above and beyond, be confident in my work, and never give up.

Table of Contents

Abstract.....iii

Acknowledgements.....v

List of Figures.....viii

List of Tables.....xi

List of Equations.....xi

Chapter 1. Literature Review 1

1.1 Introduction.....1

1.2 Tissue Engineering.....2

1.3 Alginate Hydrogels.....3

1.4 Drug Delivery using Porous Silicon.....7

1.5 Porous Silicon Structure and Fabrication Methods.....9

1.6 Porous Silicon Physically Entrapped in Alginate Hydrogels.....13

1.7 Curcumin.....14

1.8 Rhodamine.....16

Chapter 2. Methods of Loading Porous Silicon and Fabricating Alginate Hydrogels.....17

2.1 Loading Porous Silicon Nanoparticles.....18

2.2 Loading Porous Silicon Membranes.....19

2.3 Fabrication of Alginate Hydrogels.....20

2.4 Alginate Hydrogels containing Porous Silicon Nanoparticles.....22

2.5 Alginate Hydrogels containing Porous Silicon Membranes.....24

2.6 Swelling of Alginate Hydrogels.....25

Chapter 3. Release Profiles of Curcumin from Porous Silicon.....26

3.1 Curcumin Calibration Curves.....26

3.2 Encapsulation Efficiency of Curcumin in Porous Silicon.....28

3.3 Curcumin Release from Porous Silicon Nanoparticles in Water.....31

Chapter 4. Release Profiles of Rhodamine from Porous Silicon and Alginate Hydrogels.....32

4.1 Rhodamine Calibration Curves.....32

4.2 Encapsulation Efficiency of Rhodamine in Porous Silicon.....35

4.3 Rhodamine Release from Porous Silicon Nanoparticles and Alginate Hydrogels.....36

4.4 Rhodamine Release from Porous Silicon Membranes and Alginate Hydrogels.....41

Chapter 5. Conclusions and Future Work.....44

References.....46

List of Figures

Figure 1. The process of Tissue Engineering.....2

Figure 2. Structural formula of sodium alginate and alginic acid.....4

Figure 3. Schematic depiction of methods of crosslinking alginate.....5

Figure 4. Different blocks of alginate bonded with 1→4 glycosidic linkages.....6

Figure 5. Schematic illustration of the combined internal gelation of alginate crosslinked with calcium and MCO. D: glucosamine; M: mannuronate unit; G: guluronate unit; GDL: D-glucono-δ-lactone.....6

Figure 6. Egg box structure which formed in alginate polymer in the presence of cation Ca^{2+}.....7

Figure 7. A comparison of conventional drug delivery profile (consisting of an initial burst release) versus a controlled drug release profile (consisting of a sustained release), in which *c* is drug concentration and *t* is time.....9

Figure 8. Routes to porous silicon via solid silicon.....10

Figure 9. Preparation of porous Si particles by electrochemical "lift-off".....11

Figure 10. Illustration of the magnesiothermic reduction process to produce porous silicon from silica.....12

Figure 11. Structure of curcumin.....14

Figure 12. Structure of rhodamine 6G (R6G).....16

Figure 13. Fluorescence spectrum of rhodamine B in ethanol recorded at different concentrations.....17

Figure 14. 2 mg/mL R6G in ethanol.....18

Figure 15. 20 mg pSi nanoparticles being loaded with 2 mg/mL R6G in ethanol solution.....18

Figure 16. Box and tube loading methods for pSi membranes.....19

Figure 17. Empty mold constructed for alginate hydrogel fabrication.....20

Figure 18. Humidity box.....21

Figure 19. Alginate hydrogel after removal from humidity box and mold.....22

Figure 20. R6G-loaded pSi nanoparticles in alginate hydrogel reagents prior to gelation.....22

Figure 21. R6G-loaded pSi nanoparticles physically entrapped in alginate hydrogels.....23

Figure 22. Dehydrated hydrogel containing R6G-loaded pSi nanoparticles.....23

Figure 23. R6G-loaded pSi membranes physically entrapped in alginate hydrogels.....24

Figure 24. Dehydrated hydrogel containing a R6G-loaded pSi membrane.....24

Figure 25. Absorbance spectra of curcumin in ethanol and water.....26

Figure 26. Curcumin calibration curve in ethanol and water at 350 nm.....27

Figure 27. Curcumin calibration curve in ethanol and water at 420 nm.....27

Figure 28. Absorbance spectra of curcumin in DMSO.....29

Figure 29. Calibration curve of curcumin in DMSO at 420 nm.....29

Figure 30. Representative absorbance spectra of curcumin extraction in DMSO (Trial 1).....30

Figure 31. Average cumulative percent release of curcumin from pSi nanoparticles in water.....32

Figure 32. Fluorescence spectra of R6G in water at medium voltage.....33

Figure 33. Fluorescence spectra of R6G in water at high voltage.....33

Figure 34. Calibration curve of R6G in water at medium voltage at 555 nm.....34

Figure 35. Calibration curve of R6G in water at high voltage at 550 nm.....34

Figure 36. Fluorescence spectra of R6G in DMSO at medium voltage.....35

Figure 37. Calibration curve of R6G in DMSO at medium voltage at 568 nm.....36

Figure 38. Average cumulative release of R6G from pSi nanoparticles in water.....37

Figure 39. Alginate hydrogels containing R6G during release in water.....39

Figure 40. Average cumulative release of R6G from alginate hydrogels in water.....39

Figure 41. Alginate hydrogels containing R6G-loaded pSi nanoparticles during release in water.....39

Figure 42. Average cumulative release of R6G-loaded pSi nanoparticles physically entrapped in alginate hydrogels in water.....40

Figure 43. Comparison of R6G release in water from pSi nanoparticles only, alginate hydrogels only, and pSi nanoparticles physically entrapped in alginate hydrogels.....41

Figure 44. Alginate hydrogels containing R6G box-loaded pSi membranes during release in water.....42

Figure 45. Alginate hydrogels containing R6G tube-loaded pSi membranes during release in water.....43

Figure 46. Average cumulative release of R6G box and tube loaded pSi membranes physically entrapped in alginate hydrogels.....44

List of Tables

1. Swelling of six representative hydrogels.....25

List of Equations

1. Magnesiothermic reduction of silica to silicon.....12

2. Swelling ratio (Q) of alginate hydrogels.....25

3. Encapsulation efficiency.....28

Chapter 1. Literature Review

1.1 Introduction

Tissue engineering is a process that aims to repair and regenerate tissues that have been damaged by disease or injury through adhering to the body's extracellular matrix.[1] Recent advances in this field have demonstrated that biocompatible materials, such as alginate hydrogels, are an inexpensive and environmentally friendly way to achieve healing.[2] Therapeutic drugs such as growth factors can be loaded into alginate hydrogels to stimulate proliferation of the surrounding tissues. Additionally, nanostructured materials have been proved to be a safe and effective method of delivering drugs in specific medical applications. Specifically, porous silicon (pSi) is a biocompatible, biodegradable, and non-toxic material that has varying pore sizes and tunable surface chemistries, which allow it to deliver loaded drugs with varying release profiles.[3]

The main goal of this thesis project is to entrap pSi nanoparticles in alginate hydrogels, to create a two-system drug delivery mechanism specific for potential use in tissue engineering applications. Two model dyes, curcumin and rhodamine, were loaded into pSi nanoparticles to observe their release from both the pSi and alginate hydrogel. Curcumin was initially found to be too hydrophobic of a drug to achieve sufficient loading, so the release of rhodamine was observed next. The pSi nanoparticles were physically entrapped in the alginate hydrogels in a method that resulted in almost no localization, and therefore pSi membranes were loaded and inserted into the pre-gelled alginate hydrogels instead. This localization of pSi is important to control spatial delivery of the loaded molecules.

1.2 Tissue Engineering

Tissue engineering aims to repair and regenerate damaged or diseased tissues in the human body by combining the body's cells with synthetic scaffolds that promote proliferation of new tissues (**Figure 1**).[4] Treatments such as autografts, where tissue is transplanted from one site to another on a patient, is expensive and painful. Additionally, treatments such as transplants or allografts have an associated risk of rejection or infection for both the donor and recipient. A promising alternative to these treatment options is tissue engineering, which uses biological substitutes to regenerate damaged tissues instead of replacing them.[1]

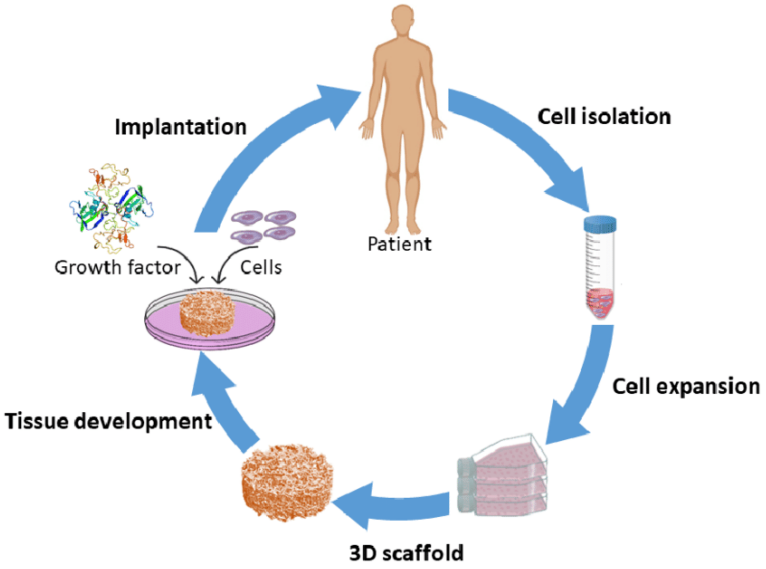

Figure 1. The process of tissue engineering.[4]

There are a variety of scaffold materials that can be used for tissue engineering applications. However, there are five of important characteristics that are necessary for these materials to have. First, the scaffolds used in tissue engineering need to be biocompatible.[1] Biocompatibility consists of the body's cells adhering to the scaffold and proliferating as they would when functioning normally. Additionally, it is critical that the scaffolds used do not cause a severe inflammatory response that would hinder healing or result in rejection by the body.[1] The next characteristic a

scaffold must have to be effective in tissue engineering is biodegradability. Biodegradability is necessary as scaffolds are not intended to be permanent.[1] Rather, they must degrade over time into non-toxic materials that are able to leave the body without interfering with the functioning of other processes. The breakdown of scaffolds overtime allows the body's cells to produce their own extracellular matrix. Other characteristics that are important for tissue engineering scaffolds to possess are specific mechanical properties that are consistent with the anatomical site where it will be implanted.[1] Tissue engineering scaffolds must contain a balance between having a strong enough mechanical integrity to function and having room to remodel as new tissues proliferate. Next, tissue engineering scaffolds must have an architecture of interconnected porosity that results in cellular penetration and adequate diffusion to surrounding cells.[1] The last important characteristic these scaffolds must have to be effective in the field of tissue engineering is affordability. In order to reach clinical and commercial use, tissue engineering scaffolds need to be cost-effective and able to be fabricated in a research laboratory in a process that can be scaled up for mass production.[1]

1.3 Alginate Hydrogels

Alginates are the second most abundant biopolymer available after cellulose, and they are extracted from various species of brown seaweeds such as *Laminaria*, *Macrocystis*, *Sargassum*, *Ascophyllum*, *Lessonia*, *Eclonia*, and *Durvillea*.[5] Commercial alginate is an anionic polymer that is normally treated with sodium or calcium chloride upon extraction from brown algae.[6] It can be treated with dilute hydrochloric acid (HCl) to be transformed into alginic acid (**Figure 2**).[5]

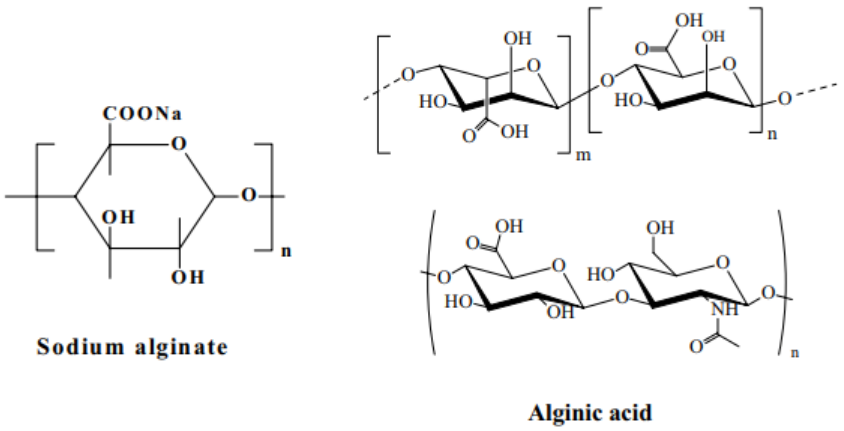

Figure 2. Structural formula of sodium alginate and alginic acid.[5]

In the US, 6.5 million patients are severely affected by chronic wound infections.[5] Additionally, over 18% of diabetic patients over the age of 65 experience foot ulcers that are not easily healed.[5] Wound dressings using alginate are more beneficial than a traditional gauze dressing for many reasons. First, alginate allows the exudates from the wound to be easily evaporated without the subsequent entry of other pathogens. Additionally, dry alginate gels can absorb fluids produced from the wound to re-gel, and the re-swelled gel in turn provides water to the dry wound to maintain a moist environment that reduces infection due to bacterial activity at the wound site.[5] Also, the extracellular matrix (ECM) that forms during proper and rapid healing of a wound will be adhered to the alginate hydrogel in the wound.[5] In hydrogel form, alginate mimics the extracellular matrices of living tissues, proving it to be useful in drug delivery, wound healing, and tissue engineering applications.

Since alginate is nontoxic, biocompatible, and biodegradable, it is rendered beneficial for various applications in industry, medical, and pharmaceutical fields.[2] Additionally, alginate has free carboxyl and hydroxyl groups along the backbone that can participate in chemical bonding, coating, and physical or chemical crosslinking.[2] These modifications allow the solubility,

reactivity, and hydrophobicity of alginate to be varied. In terms of crosslinking, there are specific types that vary the properties of alginate, which are shown in (**Figure 3)**.[2]

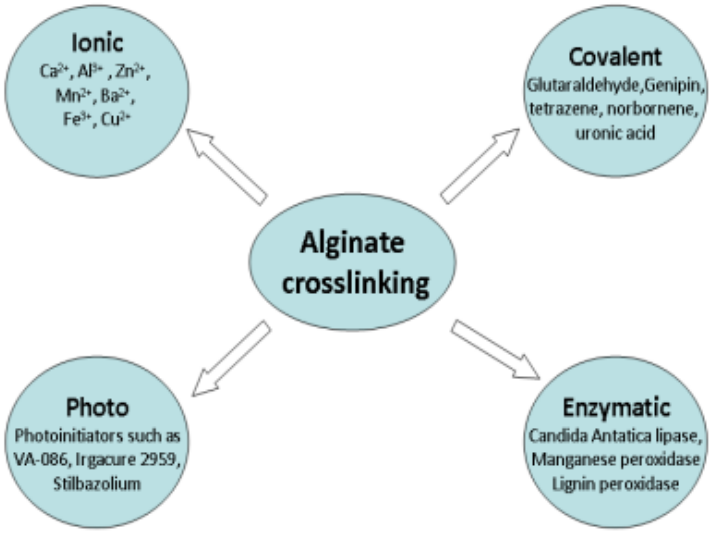

Figure 3. Schematic depiction of methods of crosslinking alginate.[2]

Alginate is considered a block copolymer of mannuronic acid (M) and guluronic acid (G) residues. The regions of alginate range from M regions, G regions, and an alternating arrangement of M and G regions.[2] This linkage is demonstrated below in **Figure 4**.[5] The regions consisting of various M and G blocks and their corresponding ratios contribute to the properties of alginate between various species of seaweed. Since only the G blocks of alginate participate in the crosslinking with divalent cations, the ratio of M/G blocks in alginate from various species of seaweed contributes to the resulting strength of the alginate hydrogel.[2]

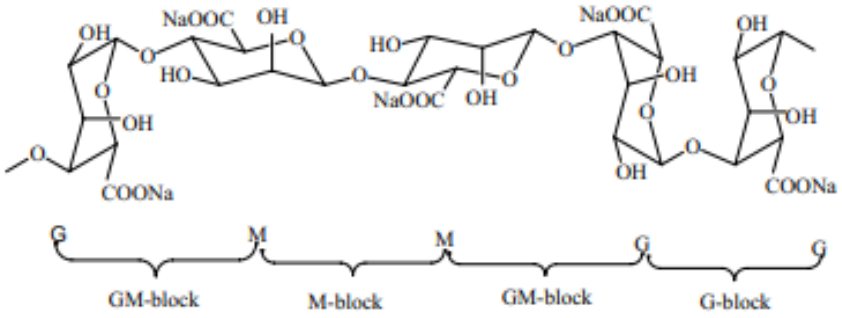

Figure 4. Different blocks of alginate bonded with 1→4 glycosidic linkages.[2]

The most straightforward method of crosslinking is ionic crosslinking, which is used to create alginate hydrogels, films, fibers, and particles. In the presence of multivalent cations such as calcium ions (Ca^{2+}), alginate can be ionically crosslinked through the G blocks.[7] The internal gelation method of preparation of alginate hydrogels occurs when a calcium salt such as calcium carbonate ($CaCO_3$) or calcium chloride ($CaCl_2$) is mixed with an alginate solution, followed by the addition of a slowly hydrolyzing proton donor that lowers the pH such as glucono-δ -lactone (GDL) to release the Ca^{2+} to form interactions with the G blocks of the alginate.[7] Furthermore, the use of a mixed chitosan oligomer (MCO) has been discovered to weakly form junctions with the M blocks of the alginate to enhance stability of the alginate hydrogel. This method is depicted in the schematic image in (**Figure 5)**.[7]

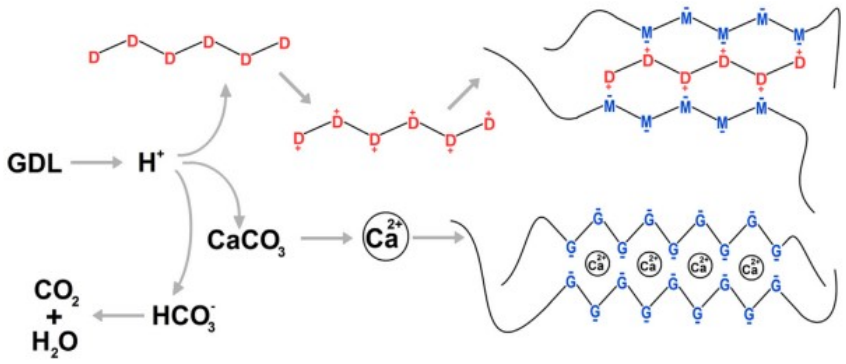

Figure 5. Schematic illustration of the combined internal gelation of alginate crosslinked with calcium and MCO. D: glucosamine, M: mannuronate unit, G: guluronate unit, GDL: D-glucono-δ-lactone.[7]

Alginate hydrogels crosslinked with Ca^{2+} form a structure known as the eggbox model (**Figure 6**)[9], which results in a property of water retention and encapsulation of various drugs or materials.[8]

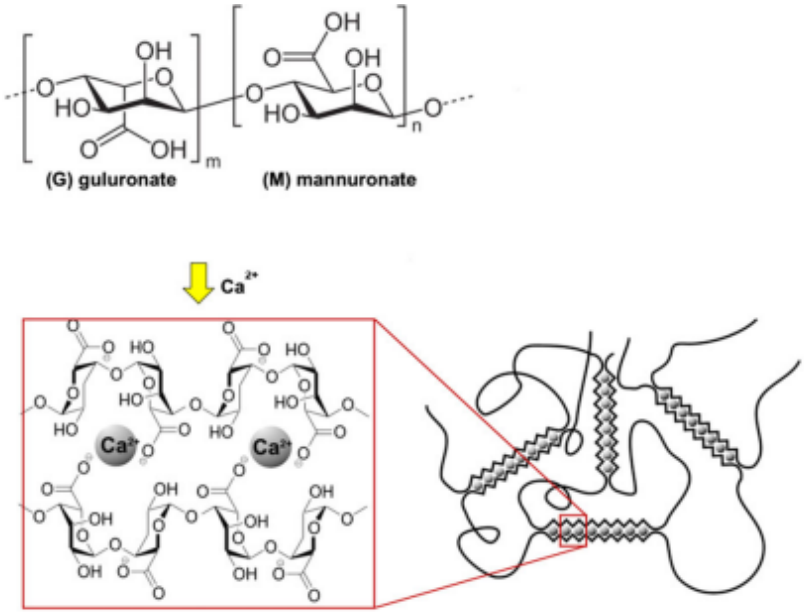

Figure 6. Egg box structure which formed in alginate polymer in the presence of cation Ca^{2+}.[9]

Some disadvantages to alginate hydrogels are that they have a difficult to control gelation rate, the structure that results if often not uniform, and it is hard to achieve the desired mechanically strong and complex-shaped three-dimensional structures.[10] It has been found that slower gelation rates result in mechanically stronger and more uniform gels.

1.4 Drug Delivery using Porous Silicon

A drug is a chemical substance delivered to the body for medical therapy. Nanotechnology and nanostructured materials are continually being investigated in the field of drug delivery to improve

safety and efficacy. Porous silicon (pSi) has proven to be biocompatible, bioresorbable, and nontoxic, rendering it a promising candidate to improve drug delivery.[3] Within the body, the dissolution rate of pSi ranges from hours to days and is dependent upon the degree of porosity, therefore influencing Si skeletal thickness and surface chemistry.[3] This tunable pore size and ability to change its surface chemistry allows for varying release profiles of the that can be adapted to a desired pharmacokinetic target. It is beneficial to use pSi in drug delivery because it is possible to load up to 45 weight percent (wt%) of a drug into this material.[3] Loading of pSi can be done at room temperature with mild solvents, indicating that it is a relatively simple process. pSi degrades to monomeric silicic acid in the body, which happens to be the most bio-available form of silicon.[3] To date, pSi has been utilized to deliver drugs orally, intravitreally, subcutaneously, intramuscularly, and intravenously.[3]

The first use of pSi in oral drug delivery was in 2003, where microfabricated pSi particles demonstrated to enhance insulin permeability across an in vitro model of human small intestinal mucosa.[3] It was observed that there was a 50-fold flux of insulin across the representative cell monolayer when using pSi in comparison to the liquid formulations with permeation enhancers (chemicals that increase drug flux through skin barriers).[3] Furthermore, it was discovered that pSi has beneficial pharmacokinetics in comparison to other drug candidates that are poorly soluble in the intestinal lumen or poorly permeable in the gastrointestinal (GI) tract.[11] Because the pores restrict the formation of the crystalline material, the amorphous state and high surface area of pSi allows the loaded drugs to have a higher dissolution rate than their crystalline counterparts.[11]

Various release profiles of drugs have been studied in attempt to enhance controlled release at the target location. A sustained release profile is the most beneficial for targeted drug release over days, weeks, months, or even years, as it reduces both the amount of drug necessary to provide the

desired therapeutic effects and the frequency of dosing[12] (**Figure 7**).[13] However, in many situations, a burst release normally occurs, where a large amount of drug is released in a short period of time before the rate of release reaches a stable profile (**Figure 7**).[13] Although a burst release has potential in certain situations to provide an instant relief followed by continued gradual treatment, there are often deleterious side effects that can result from this type of release profile.

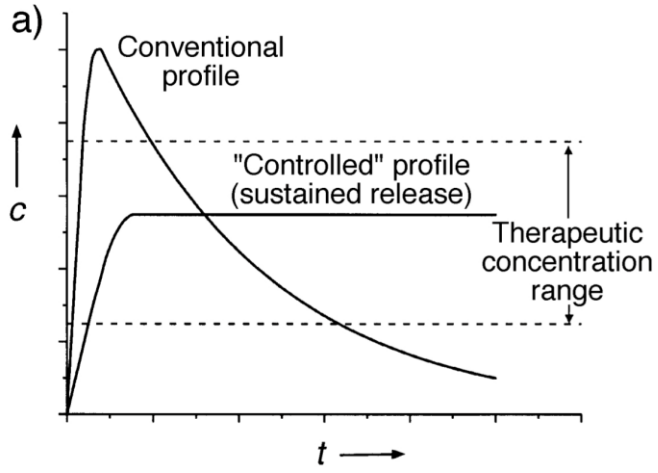

Figure 7. A comparison of conventional drug delivery profile (consisting of an initial burst release) versus a controlled drug release profile (consisting of a sustained release), in which *c* is drug concentration and *t* is time.[13]

1.5 Porous Silicon Structure and Fabrication Methods

Nanoporous silicon encompasses physical forms such as nanoparticles, nanowires, nanocomposites, membranes, ultrathin films, multilayers, superlattices, needles, and suspensions.[14] There are various routes of formation that either start with solid silicon, (**Figure 8**)[14] i.e. “top-down” methods, or alternatively, start with silicon atoms, i.e. “bottom-up” methods.[14] Each method has a wide range of applicability depending on the desired use of the nanoporous silicon that results.

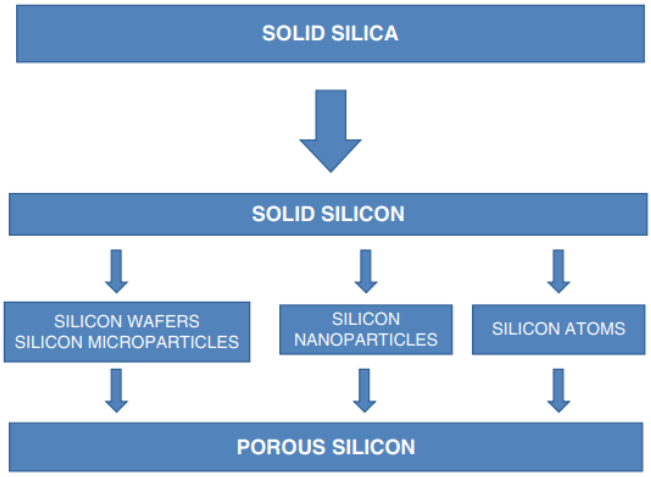

Figure 8. Routes to porous silicon via solid silicon.[14]

The pore size that results from these processes varies greatly. Microporous silicon identifies porous silicon that contains less than 2 nanometers of pore diameter.[14] Mesoporous silicon has pore sizes ranging from 2-50 nanometers in diameter.[14] These pores are mostly interconnected or branched. Macroporous silicon consists of any pore sizes larger than 50 nanometers in diameter.[14] Microporous, mesoporous, and macroporous silicon are all specific types of nanoporous silicon, which includes all three of the above types under a 100 nm pore diameter. Each type of porous silicon has a varying internal surface area. In general, as the pore size decreases, the internal surface area increases.[14] Microporous silicon has the highest internal surface area, whereas macroporous silicon has the smallest internal surface area.[14]

In addition to the varying diameter of pore sizes between batches of porous silicon, there are also differences in the accessibility of the pores. Some of the shapes that different pores have are blind (bead-end) pores, interconnected (branched) pores, closed (totally isolated pores), and penetrating pores.[15] Another complementary semiquantitative physical property of pSi is the degree of porosity within each batch. Considering porosity as percent void volume within a given structure, low porosity consists of batches with 0-30% pores, medium porosity has between 30-

70% pores, high porosity has between 70-90% pores, and ultrahigh porosity has between 90-100% pores.[15]

There are three main processes for the fabrication of pSi: (1) electrochemical etching of silicon, where the oxidant is supplied through an electrochemical current; (2) stain etching of silicon, where the oxidant is supplied through a chemical; (3) chemical reduction of silica to silicon through magnesiothermic reduction with an electropositive metal such as magnesium.

One of the best means to prepare porous silicon with controlled pore size and porosity is electrochemical etching. This process most often consists of a copper sheet as the anode and a platinum sheet as a cathode and uses hydrofluoric acid (HF) as the electrolyte solution. To make nanoparticles from this electrochemically etched pSi, the porous layer is removed from the crystal silicon substrate through a process called "lift-off" (**Figure 9**)[16] that utilizes a high current pulse or a low concentration of HF to create an undercut.[16] The undercut, or fragile layer of silicon beneath the porous layer, is then easily fractured to remove the pSi from the silicon wafer. These pSi membranes can be further fractured into pSi nanoparticles through ball milling, physical grinding, or ultrasonication.[16]

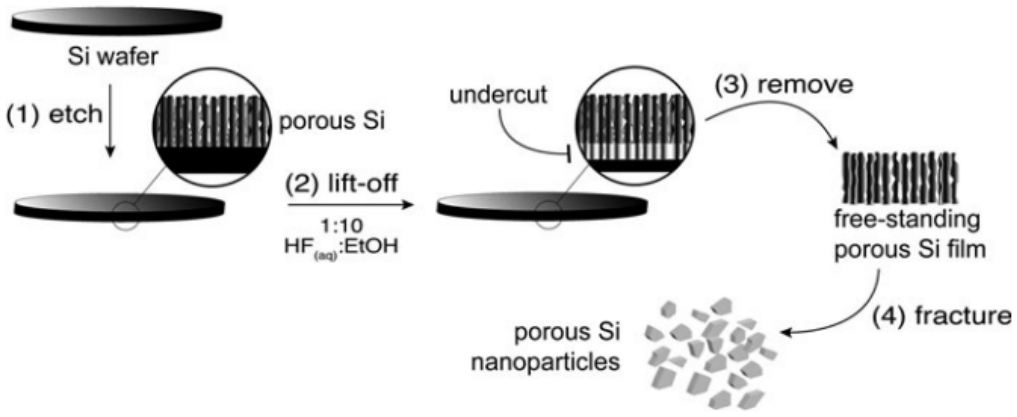

Figure 9. Preparation of porous Si particles by electrochemical "lift-off."[16]

Another method of preparation of pSi is magnesiothermic reduction, which produces pSi from the reduction of silica (SiO_2) with electropositive metals such as magnesium.[17] Magnesiothermic reduction is beneficial because it can be carried out at lower temperatures than the conventional reduction methods, allowing for the preservation of the intricate features of silicon structures. The reaction for the process of magnesiothermic reduction is shown below.[17]

$$SiO_2(s) + 2\,Mg(s) \rightarrow Si(s) + 2\,MgO\,(s) \quad \textbf{(1)}$$

After the magnesium oxide is removed with hydrochloric acid (HCl), the silicon left behind has a higher surface area than the original template. A visual diagram of the overall process of magnesiothermic reduction from silica to silicon is depicted below in **Figure 10**.[17] However, the time spent reducing varies depending upon the exact procedure utilized throughout the process.

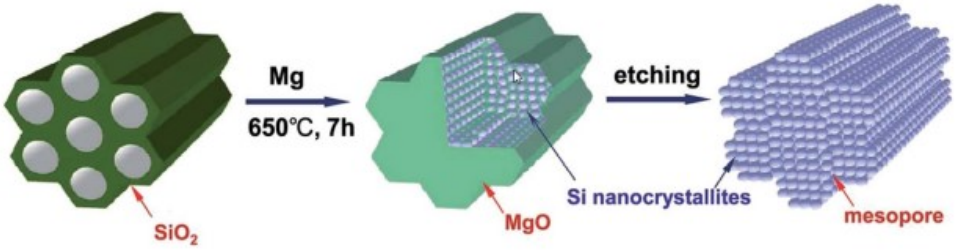

Figure 10. Illustration of the magnesiothermic reduction process to produce porous silicon from silica.[17]

In this project, both pSi nanoparticles and pSi membranes were loaded with a model dye and physically entrapped in alginate hydrogels. As will be discussed in the results, physical entrapment of pSi nanoparticles in alginate hydrogels was attempted first and was followed by the physical entrapment of pSi membranes in alginate hydrogels. Although the pore sizes of pSi nanoparticles and membranes used in this project were similar, it is important to note that the internal surface

area of the pSi nanoparticles is much larger than that of the pSi membranes, which relates to the amount of model dye that can be loaded into their pores.

1.6 Porous Silicon Physically Entrapped in Alginate Hydrogels

Alginate hydrogels have been used previously as templates for iron oxide, gold, or silver nanoparticles, which allows the size distribution of these inorganic nanoparticles to be controlled.[8] Additionally, it was found that encapsulation of nanoparticles within alginate hydrogels influences the mechanical properties of the resulting gels. Rescignano et. al found a larger elastic modulus with an alginate hydrogel loaded with silver nanoparticles (AgNPs) compared to a plain alginate hydrogel, which they concluded to reinforce the alginate network.[8] However, they also found that higher concentrations of nanoparticles contributed to a decrease in elastic modulus and a weakening in the elastic response of the alginate hydrogels.[8] This finding was attributed to the possibility of the presence of AgNPs to prevent the formation of crosslinking points along the alginate chains, resulting in a lower strain required to disrupt the network. Overall, the authors concluded that a concentration of 2.5% w/w was considered to have the most improved elastic moduli compared with concentrations of 5% and 7.5% w/w AgNPs in alginate hydrogels.[8] In this project, pSi nanoparticles were physically entrapped in alginate hydrogels at a concentration lower than 1% w/w, which not only allowed for an enhanced visual of the loaded dye diffusing out during release, but also ensured that no hinderance of alginate crosslinking would occur during gel formation.

1.7 Curcumin

The first dye that was chosen to load into pSi was curcumin, which is a relatively water insoluble model drug that can be both quantitatively measured through UV/vis spectroscopy and qualitatively through the observation of color.

Water-soluble drugs normally display fast release profiles in drug delivery, while poorly soluble drugs exhibit slower release kinetics.[3] The poorly soluble curcumin dye, therefore, was thought to be a model that would result in a more sustained release profile when monitoring release in an aqueous environment. Additionally, its potential therapeutic effects rendered it a beneficial model dye to test the efficiency of the pSi/alginate release system.

Curcumin (diferuloylmethane) is the major component of the widely used spice turmeric (*Curcuma longa*) and contributes to its yellow color.[5] Curcumin (**Figure 11**) has been shown to exhibit a broad range of therapeutic effects like anti-inflammatory, anticarcinogenic, antioxidant, and anti-infective properties, which suggest it can accelerate the process of wound healing.[5] Although the main use of curcumin is as a spice, it has also been used for herbal medicines to treat diseases such as rheumatism, anorexia, sinusitis, diabetic ulcers, and cough.[5]

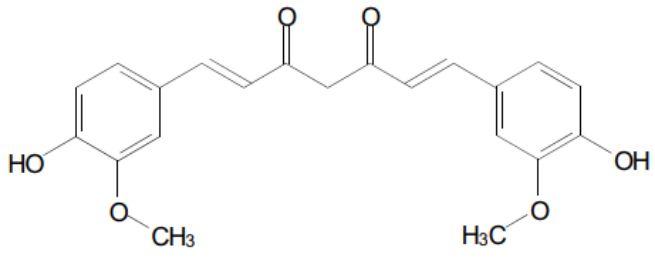

Figure 11. Structure of curcumin.

The main reason curcumin is extensively studied for therapeutic applications are its low level of toxicity when consumed by humans. However, there are some known shortcomings of curcumin such as poor aqueous solubility and low bioavailability in the human body.[19] The main reasons that an agent in the body has low bioavailability are poor absorption, low intrinsic activity, high metabolism rate, inactivity of metabolic products, or rapid elimination and clearance from the body.[20] Recent studies have found curcumin to have poor absorption and rapid metabolism in the body, rendering it to have a reduced bioavailability.[20]

Additionally, curcumin is very hydrophobic and is therefore difficult to measure in aqueous solutions using UV/vis absorption spectroscopy.[19] However, curcumin is soluble in ethanol, and a stock solution of curcumin in ethanol can be diluted with water in order to create a calibration curve to be used in experiments with UV/Vis spectroscopy. Furthermore, curcumin is said to form aggregates and precipitate out in water, therefore contributing to its poor aqueous solubility. [21] Furthermore, curcumin is light-sensitive, so all glassware throughout this project that contained this model dye was covered in aluminum foil.

Banjeree et. al found that the absorption peaks for curcumin in water existed at 430 nm and 355 nm. The band at 430 nm is assigned to the lowest π-π* transitions in curcumin, and the peak at 355 nm with the shoulder is assigned to the π-π* transitions in the feruloyl unit.[21] Alternative spectral measurements in octanol find a peak around 350 nm present.[21] Overall, it was found that curcumin exhibits a broad absorption spectrum in aqueous solution with low intensity.

The molecular weight of curcumin used in these experiments and calculations was 368.39 g/mol.

1.8 Rhodamine

Rhodamine, with its relatively high aqueous solubility, was the second model dye chosen after it was experimentally determined that curcumin was too hydrophobic to achieve significant loading of pSi. Within the family of rhodamine dyes, two main dyes are rhodamine 6G and rhodamine B. Rhodamine 6G (**Figure 12**) is also known as Rhodamine 590 or R6G, and can exist as a chloride, perchlorate, or tetrafluoroborate salt. The chloride salt of rhodamine 6G was the specific type of dye used in this project.

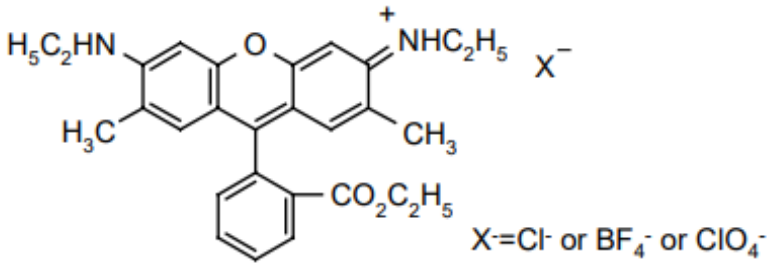

Figure 12. Structure of rhodamine 6G (R6G).

Rhodamine dyes appear red to violet in color and are often used as tracer dyes in water to determine the rate and direction of flow and transport.[22] Some applications of rhodamine dyes in biotechnology are fluorescence microscopy, flow cytometry, fluorescence correlation spectroscopy, and ELISA.[22] In the past, rhodamine dyes have also been used in various biological applications for tissue staining, binding to proteins, and photodynamic therapy.[23] Additionally, the rhodamine dye has been used to follow conformational changes among proteins.[23]

Rhodamine was chosen as a model dye due to its ability to be measured using fluorescence spectroscopy. It is important to note, however, that the various concentrations of rhodamine dyes in different solvents result in a shift in the intensity peaks measured. In Al-Kadhemy et. al, the fluorescence spectra of four concentrations of rhodamine B in ethanol were obtained

experimentally ($1x10^{-2}$, $1x10^{-3}$, $1x10^{-4}$, and $1x10^{-5}$ mol/L). Upon varying the concentrations from $1x10^{-5}$ M to $1x10^{-2}$ M, a 20 nm red shift was observed (**Figure 13**).[22] Furthermore, the intensity of the fluorescence spectrum was found to have increased with increasing concentration of the dye solution.[22]

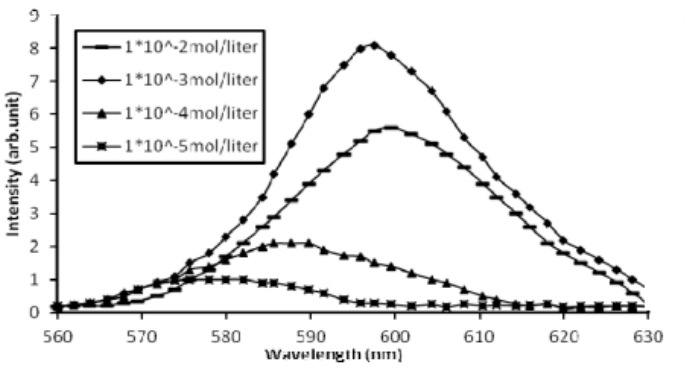

Figure 13. Fluorescence spectra of rhodamine B in ethanol recorded at different concentrations.[22]

The molar mass of R6G used in these experiments and calculations was 479.02 gm/mol.

Chapter 2. Methods of Loading Porous Silicon and Fabricating Alginate Hydrogels

The following instruments were used in this research:

- Vortex-Genie Mixer – Model: S8223, No. G11787
- Horn Sonicator – Branson Sonicator Model: 450
- VWR Incubating Orbital Shaker
- UV-Vis Spectrophotometer – Agilent Model: Cary 60
- Fluorescence Spectrophotometer – Agilent Model: Cary Eclipse
- Thermo Scientific mySPIN 12 Centrifuge
- Cole Parmer Centrifuge FS-3500

2.1 Loading of Porous Silicon Nanoparticles

The procedure for loading pSi nanoparticles was the same when using both model dyes in this project. The target mass loading of model dye into the pSi nanoparticles was around 20%. In an attempt to achieve this, a 2 mg/mL model dye solution in ethanol (**Figure 14**) was created and was added dropwise to 20 mg of pSi resting in a 10 mL beaker on a hot plate set at 37℃ to both facilitate faster evaporation of the solvent and to mimic internal body conditions (**Figure 15**). Specifically, 20 additions of 100 µL aliquots of the model dye solution in ethanol were added, and the solvent was allowed to evaporate between each addition.

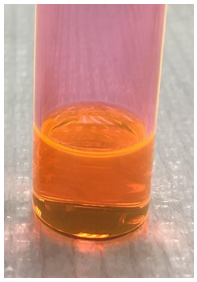

Figure 14. 2 mg/mL R6G in ethanol.

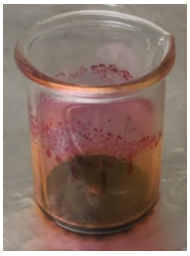

Figure 15. 20 mg pSi nanoparticles being loaded with 2 mg/mL R6G in ethanol solution.

It is important to notice in **Figure 15** above that there is dye residue located around sides of the beaker. As the solvent evaporated, some of the model dye (R6G in this scenario) was left on the sides of the beaker. Therefore, it is expected that the actual loading of this batch of pSi nanoparticles will be less than the targeted loading of 20%.

After the completion of this loading procedure, the pSi was transferred to a glass bottle and allowed to dry overnight in a vacuum. The model-dye loaded pSi nanoparticles were stored in a desiccator when not in use for experimentation.

2.2 Loading of Porous Silicon Membranes

The loading procedure for pSi membranes slightly differed from that of loading pSi nanoparticles. Two methods of loading pSi membranes were attempted. The first method was loading pSi membranes in a small plastic box lying flat on the table (**Figure 16a**) and the second method was loading pSi membranes in a small plastic tube sitting at an angle (**Figure 16b**).

16a. 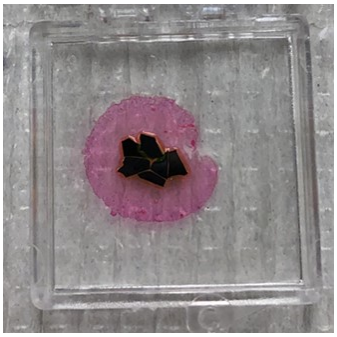 **16b.** 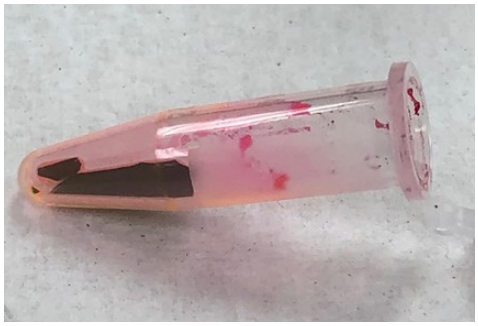

Figure 16. Box (**a**) and tube (**b**) loading methods for pSi membranes.

Both the tube-loading and box-loading methods for pSi membranes were carried out with the same procedures. First, the mass of the membrane was determined, and the volume necessary to achieve a 20% loading from a 2 mg/mL R6G in ethanol solution was calculated. Next, each addition of the model dye solution was added dropwise to the membrane, allowing for evaporation of the solvent between each addition. In the box loading method, the dye solution was added directly on top of the membrane lying flat on the table. in the tube loading method, the dye solution was added to the top of the membrane resting at a slant in the tube, allowing for the dye to seem into the pores as the ethanol evaporated off, with any additional solution collecting at the bottom

of the tube. After the completion of loading, both the box and tube were left open overnight to allow the model-dye loaded pSi membranes to dry and were stored in a desiccator when not in use for experimentation.

2.3 Fabrication Methods of Alginate Hydrogels

Rescignano et al prepared alginate hydrogels consisting of a 2% w/v aqueous alginate solution, a 10 mg/2.5 mL aqueous calcium carbonate solution, and a 0.15 g/2.5 mL aqueous GDL solution.[8] The alginate solution was left on magnetic stirring for 24 hours prior to use. To create the hydrogel, 10 mL of the alginate solution, 2.5 mL of the calcium salt solution, and 2.5 mL of the GDL were briefly stirred before sitting in a humidity box for a week to undergo gel formation.[8] For this project, the same ratio of reagents was maintained, but the volumes were downscaled to create individual alginate hydrogels in molds on 1 cm square glass slides. Additionally, calcium chloride was used instead of calcium carbonate due to availability.

In order to fabricate alginate hydrogels, the molds first were constructed by cutting plastic tube tops off using a razorblade. These molds were then hot glued onto a 1 in x 1 in glass slide that had been previously cut (**Figure 17**). The inner dimensions of the mold were measured to be around 1 cm in diameter and 1.5 cm deep.

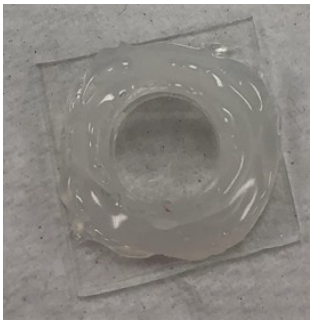

Figure 17. Empty mold constructed for alginate hydrogel fabrication.

After the molds were constructed, the three aqueous reagents necessary to make alginate hydrogels were accurately pipetted into their respective molds. First, 400 µL of 2% w/v alginate solution was added. To make this solution, sodium alginate in powder form was magnetically stirred into water for 24 hours. Next, 100 µL of a 10 mg/2.5 mL $CaCl_2$ solution was added and mixed with the alginate using the pipette tip. Finally, 100 µL of glucono-δ-lactone (GDL) was added and mixed with the other reagents using the pipette tip. GDL ($C_6H_{10}O_6$) is a slow-release acidifier that slowly hydrolyzes to gluconic acid, releasing calcium ions from the calcium salt to initiate the crosslinking of alginate without an external trigger (such as a pH change). GDL is an optimal dissociating agent for the calcium salt in alginate because it allows alginate to be poured into molds prior to its gelation.[24] Gels that were attempted to be made without adding GDL demonstrated a severe loss of film integrity, and therefore were not able to be utilized in experiments.

Once the reagents all are mixed together in their molds, they are placed in a humidity box for a week to form gels. This humidity box consists of a Styrofoam box that contains a large surface area petri dish under it filled to the top with water (**Figure 18**). Additionally, each mold is placed under a petri dish in this humidity box.

Figure 18. Humidity box.

After a week of gelation in the humidity box, the alginate hydrogels are carefully removed from their molds and allowed to completely dehydrate for future release experiments. Below, in **Figure 19**, is a picture of a plain alginate hydrogel after spending a week in the humidity box to gel and being removed from its mold.

Figure 19. Alginate hydrogel after removal from humidity box and mold.

2.4 Alginate Hydrogels containing Porous Silicon Nanoparticles

The first method of physically entrapping pSi in alginate hydrogels consisted of mixing model-dye loaded pSi nanoparticles in with the aqueous alginate solution prior to pipetting it into the molds. To achieve this, a specific mass of R6G-loaded pSi was weighed out in a 1.5 mL microfuge tube, and the 400 µL of the alginate solution was added to this small tube. The resulting pSi/alginate slurry was quickly pipetted into each mold, and then the $CaCl_2$ and GDL reagents were added before it was placed in the humidity box for a week to gel (**Figure 20**). This method was termed the "quick aqueous" method.

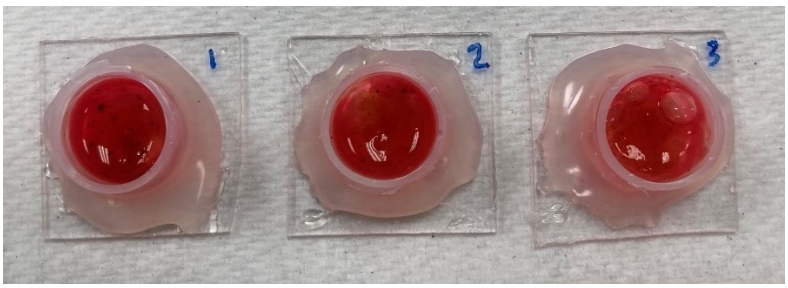

Figure 20. R6G-loaded pSi nanoparticles in alginate hydrogel reagents prior to gelation.

The main problem encountered when experimenting with the "quick aqueous" method was that R6G is very soluble in water, and therefore released very quickly from the pSi nanoparticles into the hydrogel as it was gelling for a week. The resulting hydrogels after gelling for a week in the humidity box were seen to be red for this reason, as seen below in **Figure 21**. The dark specs seen in these gels are the pSi nanoparticles distributed throughout the hydrogel.

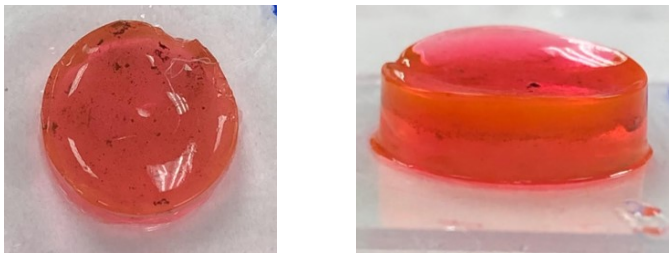

Figure 21. R6G-loaded pSi nanoparticles physically entrapped in alginate hydrogels.

These hydrogels containing R6G-loaded pSi nanoparticles were allowed to completely dehydrate prior to being used in release experiments (**Figure 22**).

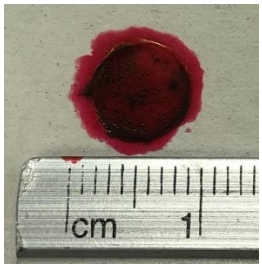

Figure 22. Dehydrated hydrogel containing R6G-loaded pSi nanoparticles.

As seen qualitatively, the quick release of R6G from the pSi nanoparticles into the hydrogel did not allow for the sustained release of the dye that was desired. Therefore, R6G-loaded pSi membranes were physically entrapped in alginate hydrogels instead of pSi nanoparticles, which have a lower surface area and ideally would slow the release of the R6G into the aqueous alginate as the hydrogel is gelling.

2.5 Alginate Hydrogels containing Porous Silicon Membranes

The second method of physically entrapping pSi into alginate hydrogels was called the "pSi membrane" method and consisted of inserting R6G-loaded pSi membranes into plain alginate hydrogels after they were gelled for a week in the humidity box and removed from their molds. After discarding the molds, a scalpel was used to slit the tops of each hydrogel open, and tweezers were used to vertically insert a R6G-loaded pSi membrane into the gel. Hydrogels containing R6G-loaded pSi membranes are shown below in **Figure 23.**

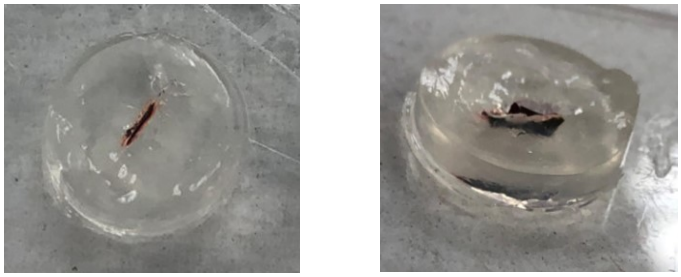

Figure 23. R6G-loaded pSi membranes physically entrapped in alginate hydrogels.

After the completion of the "gel surgery," the membrane-loaded hydrogels were allowed to completely dehydrate (**Figure 24**).

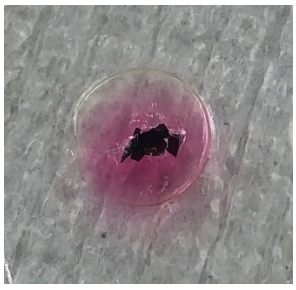

Figure 24. Dehydrated hydrogel containing a R6G-loaded pSi membrane.

This method was qualitatively shown to improve the localization of the pSi within the hydrogel, and additionally to result in a more sustained release profile of the model dye from the pSi into the hydrogel (*vide infra*).

2.6 Swelling of Alginate Hydrogels

To analyze the water retention of alginate hydrogels, the swelling ratio can be determined. After the plain alginate hydrogels successfully were gelled, they were completely dehydrated and weighed. Then, they were placed in an aqueous environment to be rehydrated for 30 minutes. In this experiment, 10 mL of deionized water was poured into a petri dish with the dehydrated gel. Then, the water was removed from the petri dish, and the gels were reweighted. The mass swelling ratio (Q) was determined using the equation below:[24]

$$Q = \frac{(W_s - W_d)}{W_d} \quad \textbf{(2)}$$

Here, W_s is the weight of the swollen hydrogel and W_d is the weight of the completely dehydrated hydrogel. From the literature values, the swollen weights range from 4,000 to 13,000 times the weights of the dry hydrogels.[24]

The swelling ratios of six representative hydrogels are shown below in **Table 1**: These representative hydrogels contained pSi nanoparticles that were not loaded with a model dye.

Hydrogel #	Mass of dry film (g)	Mass of swelled gel (g)	Swelling
1	0.0227	0.3065	12.5x
2	0.0350	0.3855	10.0x
3	0.0241	0.2998	11.4x
4	0.0267	0.3104	10.6x
5	0.0257	0.3232	11.6x
6	0.0243	0.3524	13.5x

Table 1. Swelling of six representative alginate hydrogels.

Chapter 3. Release Profiles of Curcumin from Porous Silicon

3.1 Curcumin Calibration Curves

To measure the release of curcumin from pSi nanoparticles, a calibration curve of curcumin first was created. Since curcumin is very insoluble in water, the stock solution of curcumin was made using ethanol with a solvent, and then the dilutions were carried out by adding water in proper volumes to this stock solution. The concentrations chosen for curcumin in ethanol/water were 2 µg/mL, 4 µg/mL, 6 µg/mL, 8 µg/mL, and 10 µg/mL. The resulting absorbance spectra are shown below in **Figure 25**. The path length of the cuvette used in the UV/Vis spectrophotometer was 1 cm.

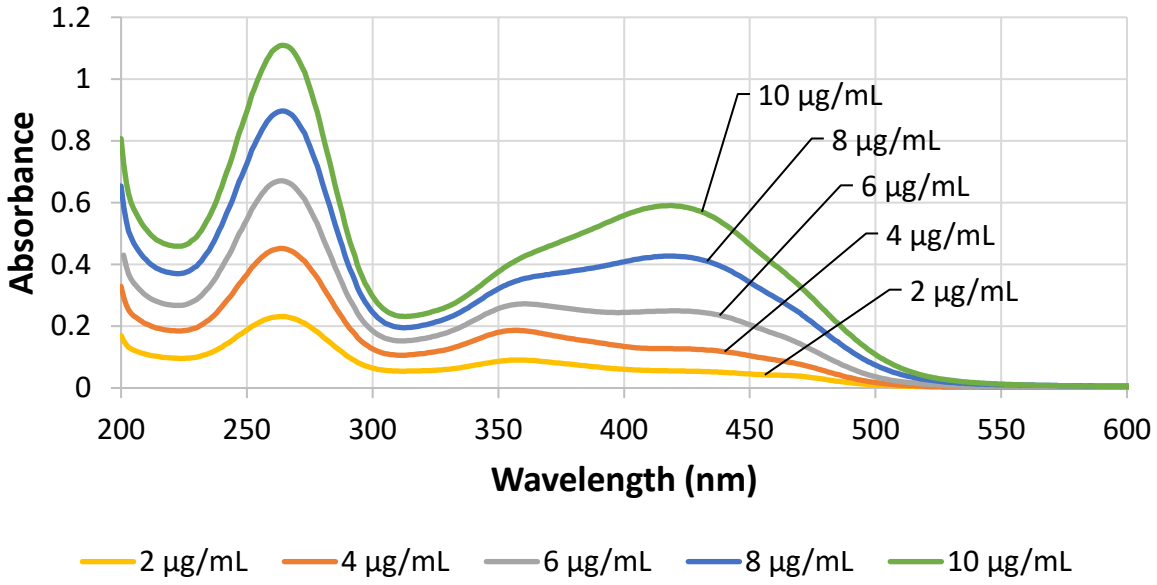

Figure 25. Absorbance spectra of curcumin in ethanol/water solutions.

The peak observed at 264 nm in **Figure 25** above was not seen when measuring the absorbance of the curcumin in water during release experiments due to blurring from the Si present in solution. Therefore, the less prominent 350 nm and 420 nm peaks were chosen to be used in calculations, since they did were not affected by Si interference. The extinction coefficient at 350 nm was 14.023

L/(mmol*cm), and the calibration curve used for calculations is shown below in **Figure 26.** The extinction coefficient at 420 nm was 22.027 L/(mmol*cm), and the calibration curve used for calculations is shown below in **Figure 27**.

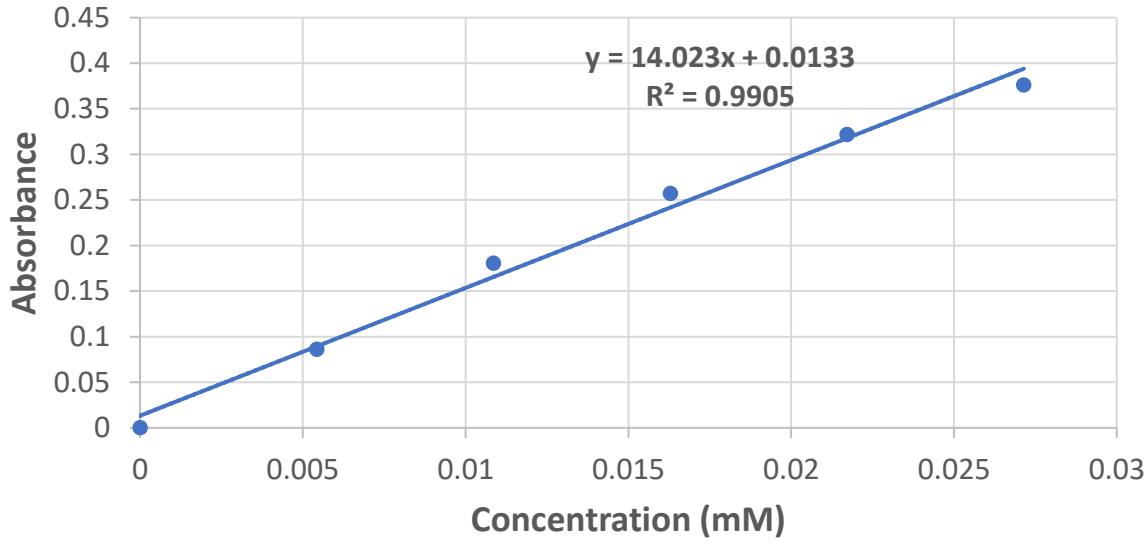

Figure 26. Curcumin calibration curve in ethanol/water mixtures at 350 nm.

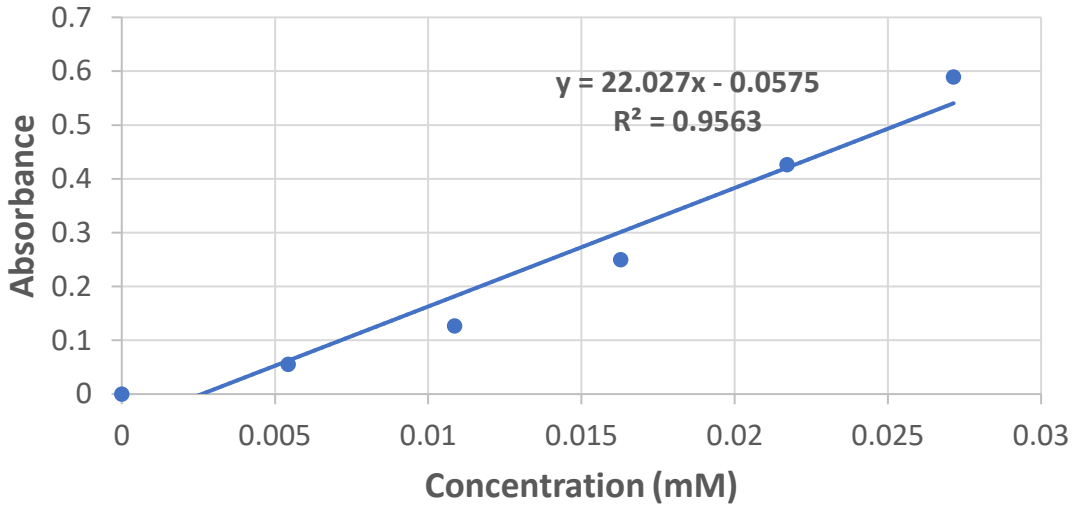

Figure 27. Curcumin calibration curve in ethanol/water mixtures at 420 nm.

3.2 Encapsulation Efficiency of Curcumin in Porous Silicon

Molecular infiltration into nanoporous channels can be challenging. Because the pore size and volume within each batch of pSi varies, the actual loading of the dye within each sample produces a range of values. Concentrating the infiltrated molecule at a given pore can result in clogging a pore, etc. Furthermore, the theoretical or maximum possible loading is rarely accomplished due to residues of the dye being deposited on the sides of the glassware used for loading, instead of seeping into the pores as the solvent evaporates. These scenarios can result in inconsistencies in the data from release procedures if not accounted for.

To account for these inconsistencies in loading, the encapsulation efficiency can be determined, which obtains a more accurate value of the actual loading of the dye in pSi through extraction of the loaded material in dimethyl sulfoxide (DMSO). A Beer's Law analysis can then be used to determine the amount of the model dye extracted and how much of the model dye was actually present within the pSi sample. The equation used for calculating the encapsulation efficiency of the model dye loaded into pSi is shown below.[25]

$$Encapsulation\ efficiency = \frac{actual\ amount\ of\ drug\ loaded}{theoretical\ (maximum) amount\ of\ drug\ loaded} \times 100\% \quad \textbf{(3)}$$

The absorbance spectra (**Figure 28**) and calibration curve (**Figure 29**) of curcumin in DMSO are shown below. The extinction coefficient for the calibration curve of curcumin in DMSO at 420 nm was calculated to be 45.31 (L/mmol*cm).

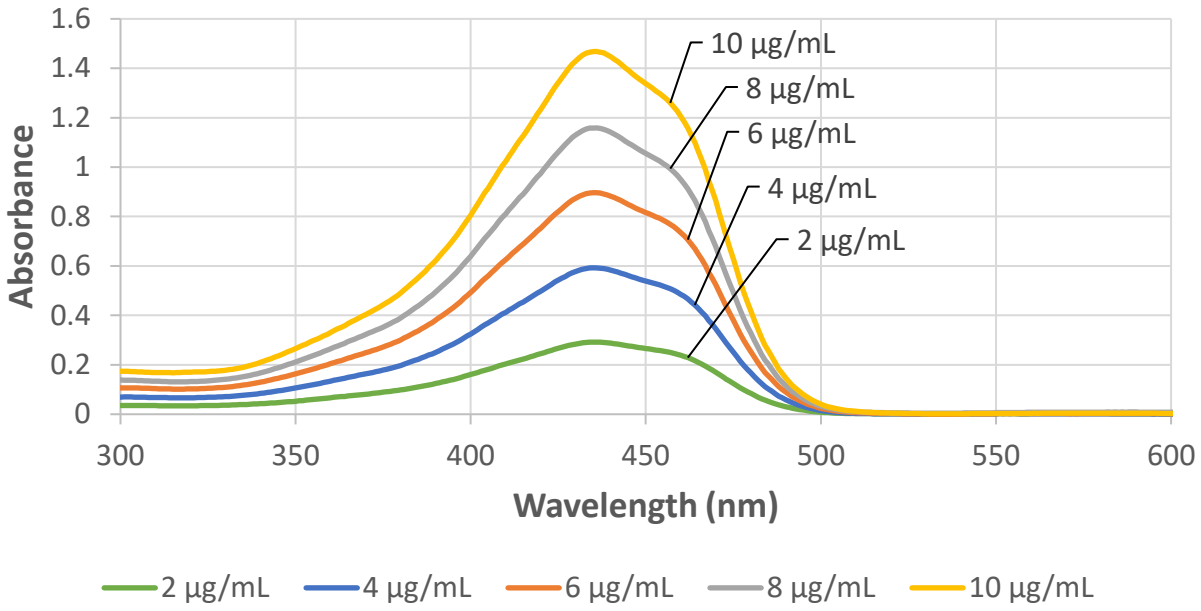

Figure 28. Absorbance spectra of curcumin in DMSO.

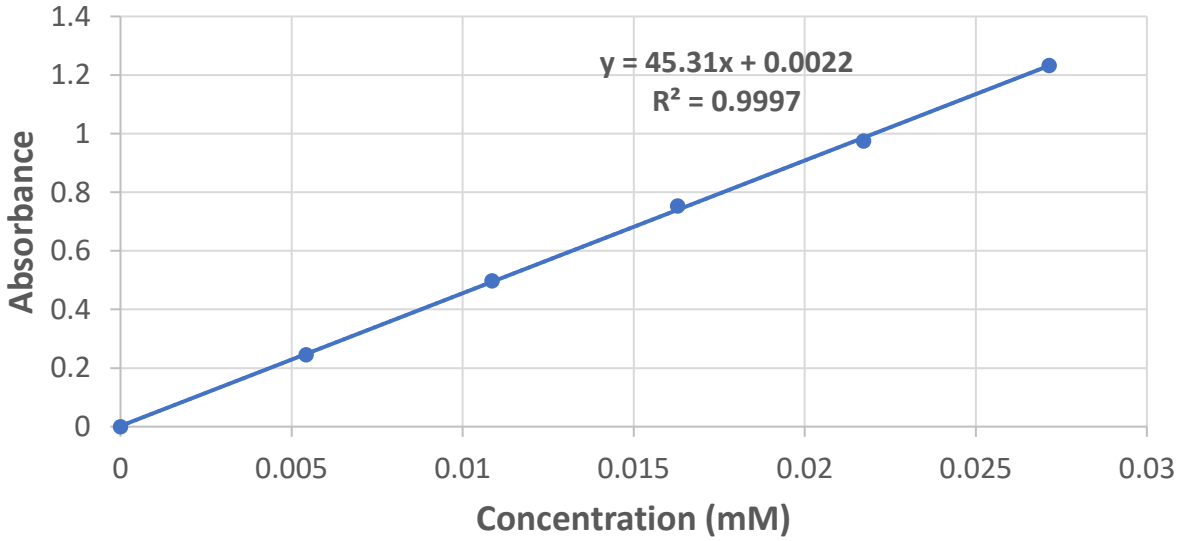

Figure 29. Calibration curve of curcumin in DMSO at 420 nm.

The procedure for determining encapsulation efficiency was similar to the release procedures. Three trials of extraction were carried out using a known mass of curcumin-loaded pSi in 2 mL plastic centrifuge tubes. Exactly 1.0 mL of DMSO was pipetted into each of these centrifuge tubes, and they were placed in a shaking incubator set at 37°C for 5 minutes. The tubes

were then placed in the Thermo Scientific mySPIN 12 centrifuge and spun at 5000 rpm for 2 minutes to allow the pSi to gather in the bottoms of the tubes. Next, a known volume of the supernatant was removed, and the absorbance was measured using the UV/Vis spectrophotometer. This process was repeated at the time intervals of 5 minutes, 10 minutes, and 20 minutes, until all the curcumin was qualitatively seen to have been released from the pSi in the centrifuge tube. The absorbance spectra for one of the three trials of extraction of curcumin in DMSO are shown below in **Figure 30**. It can be seen from these spectra that after the 20-minute time interval, all the curcumin dye was fully extracted from the pSi sample, and therefore the experiment was concluded.

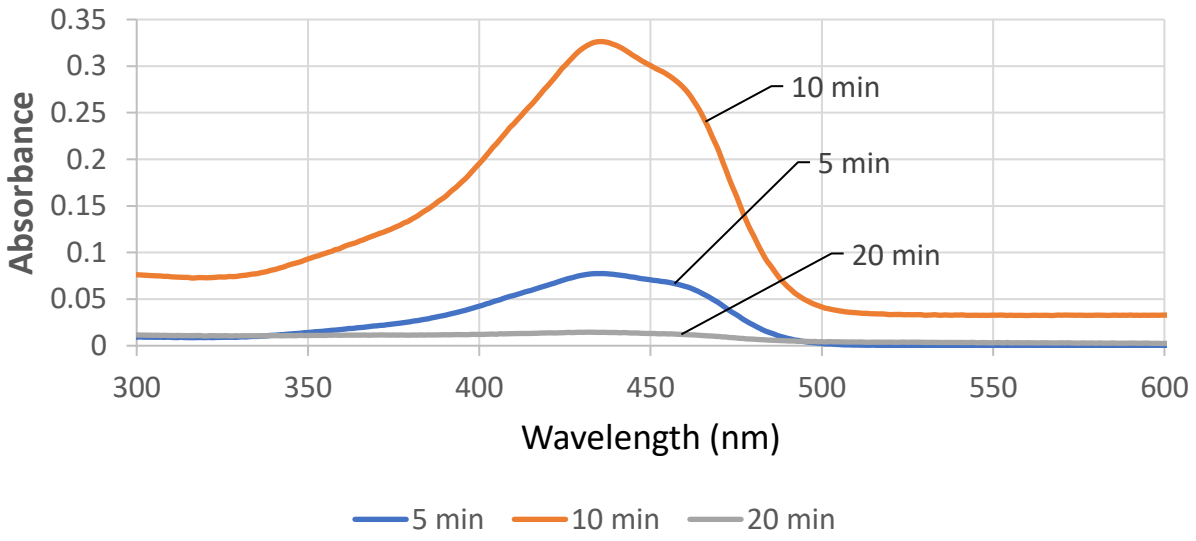

Figure 30. Representative absorbance spectra of curcumin extraction in DMSO (Trial 1).

The encapsulation efficiency calculated for curcumin loaded in pSi nanoparticles was 18.84%, which was slightly lower than the targeted 20% loading. The actual loading of 18.84% was then used to determine the mass of curcumin in the mass of pSi nanoparticles when calculating the cumulative release of the model dye in experimentation.

3.3 Curcumin Release from Porous Silicon Nanoparticles in Water

To release curcumin from pSi nanoparticles, a known amount of loaded pSi was first weighted out into three separate 2 mL plastic centrifuge tubes. Next, exactly 1 mL of water was pipetted into each of the three tubes, and they were placed in a shaking incubator set at 37℃ for each time interval. The time intervals chosen to measure the release of the model dye at were 5 minutes, 10 minutes, 20 minutes, 40 minutes, and 60 minutes. At each of these times, the trials were removed from the incubator, centrifuged for 2 minutes at 5000 rpm, and a known volume of the supernatant was removed, diluted with water if necessary, and placed in the UV/Vis spectrophotometer to measure the absorbance of the supernatant. Then, the rest of the supernatant was removed from each trial, and a fresh 1 mL of water was placed in each tube for the continuation of the experiment.

The environment and conditions of release of the model dye from pSi were determined to best align with internal body conditions. Therefore, water was used as the medium, since the body is mostly an aqueous environment, and the shaking incubator was set at 37℃, which is consistent with internal body temperature. Furthermore, since three trials were carried out in the release experiment, the results were averaged and presented in a single graph containing the average cumulative release of curcumin plotted over time. This release experiment was repeated twice, and therefore two trials of average cumulative release curves are shown in **Figure 31** below.

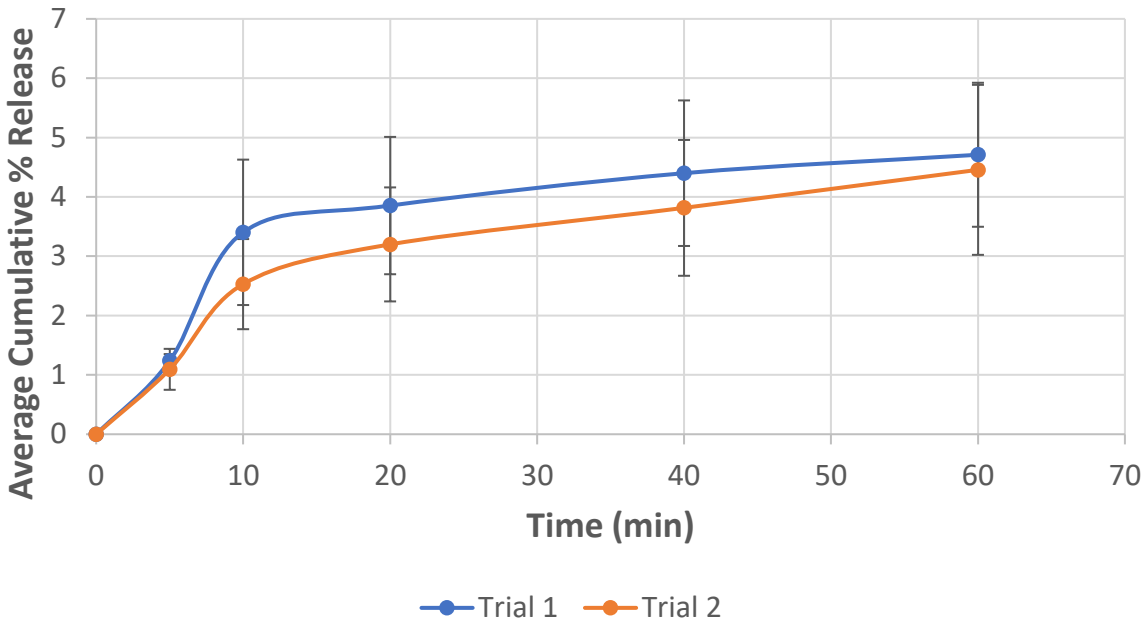

Figure 31. Average cumulative percent release of curcumin from pSi nanoparticles in water.

As seen in **Figure 31** above, both trials of curcumin release from pSi nanoparticles in water resulted in an average cumulative release of less than 5% (4.7% for Trial 1 and 4.5% for Trial 2). Therefore, it was concluded that curcumin was too hydrophobic of a drug to achieve significant loading into pSi nanoparticles, and another model dye was chosen to examine release.

Chapter 4. Release Profiles of Rhodamine from Porous Silicon and Alginate Hydrogels

4.1 Rhodamine Calibration Curves

A calibration curve of R6G in water was first created by diluting a stock solution of R6G in water to 10 µg/mL, 8 µg/mL, 6 µg/mL, 4 µg/mL, and 2 µg/mL. R6G has fluorescent properties, and therefore the intensities of each of these solutions was measured using the fluorescence spectrophotometer. One of the settings on the fluorescence spectrophotometer allows a change of voltage from medium (600 V) to high (800 V) with respect to the photomultiplier tube (PMT), which allows more sensitivity in measuring concentrations within a specified range. If the voltage is increased, it allows the intensities of a smaller amount of dye to be measured. The concentrations

used for the creation of the high voltage calibration curve of R6G in water were 0.133 µg/mL, 0.267 µg/mL, 0.400 µg/mL, 0.533 µg/mL, and 0.667 µg/mL. Intensity versus wavelength spectra were taken using the fluorescence spectrophotometer at both medium voltage (**Figure 32**) and high voltage (**Figure 33**).

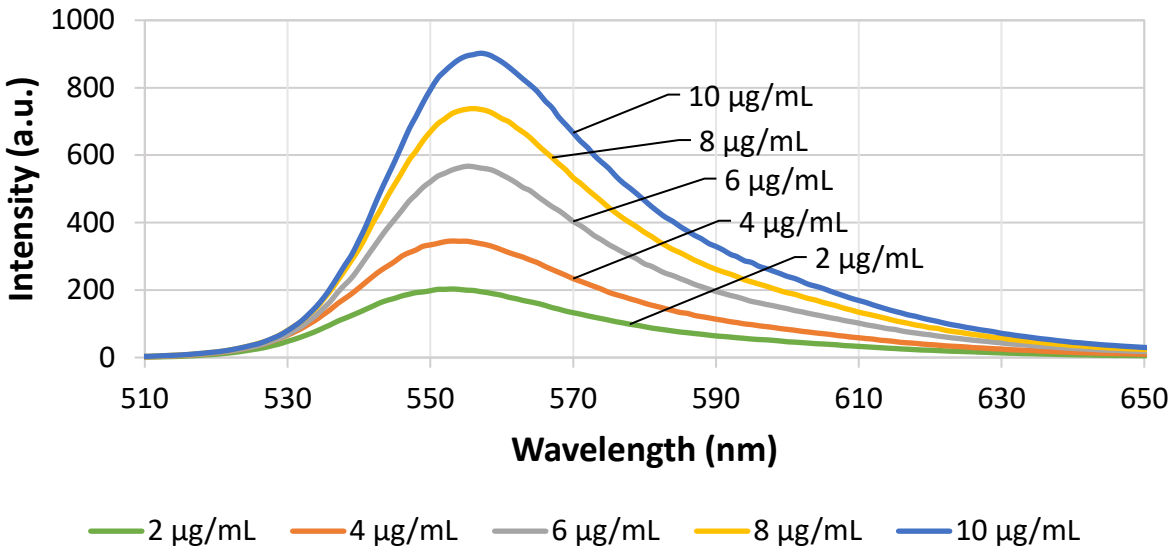

Figure 32. Fluorescence spectra of R6G in water at medium voltage.

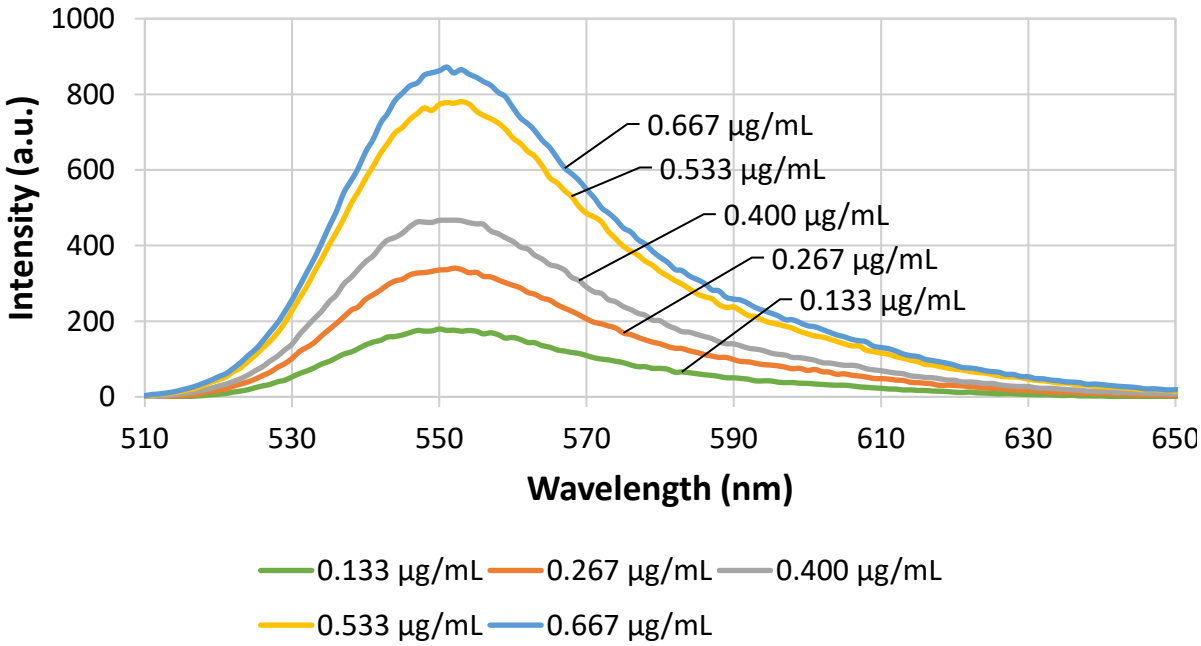

Figure 33. Fluorescence spectra of R6G in water at high voltage.

The peaks chosen from these spectra to construct the calibration curves of R6G in water were 555 nm for the medium voltage and 550 nm for the high voltage. These calibration curves are shown below in **Figures 34-35**.

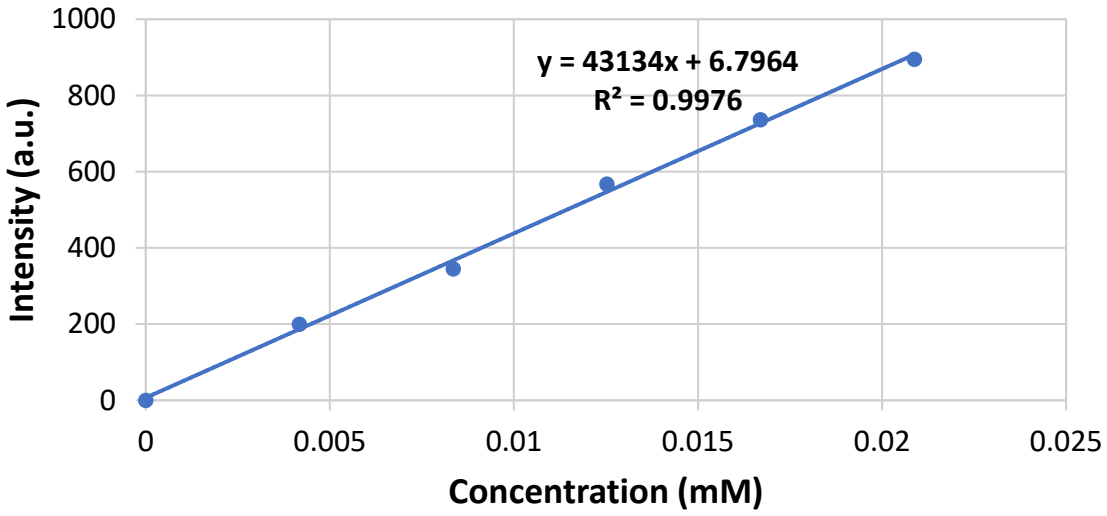

Figure 34. Calibration curve of R6G in water at medium voltage at 555 nm.

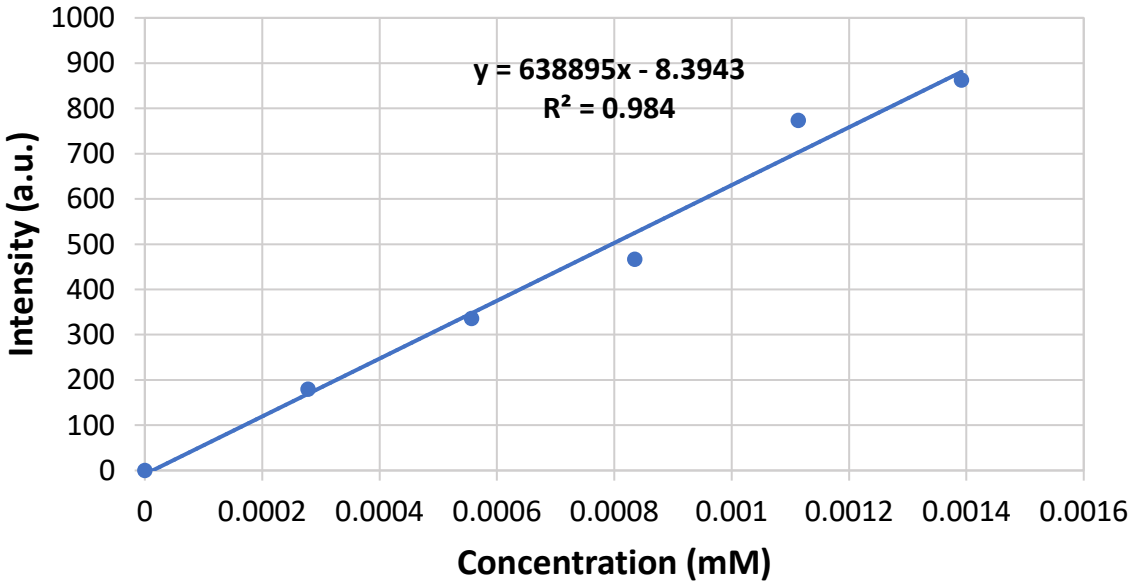

Figure 35. Calibration curve of R6G in water at high voltage at 550 nm.

4.2 Encapsulation Efficiency of Rhodamine in Porous Silicon

The encapsulation efficiency of R6G in DMSO was determined through the fluorescence spectra (**Figure 36**) and calibration curve (**Figure 37**). The concentrations of R6G in DMSO measured were 10 µg/mL, 8 µg/mL, 6 µg/mL, 4 µg/mL, and 2 µg/mL. The wavelength chosen from the fluorescence spectra to create the calibration curve from was 568 nm, and **Equation 3** was used to calculate the encapsulation efficiency.

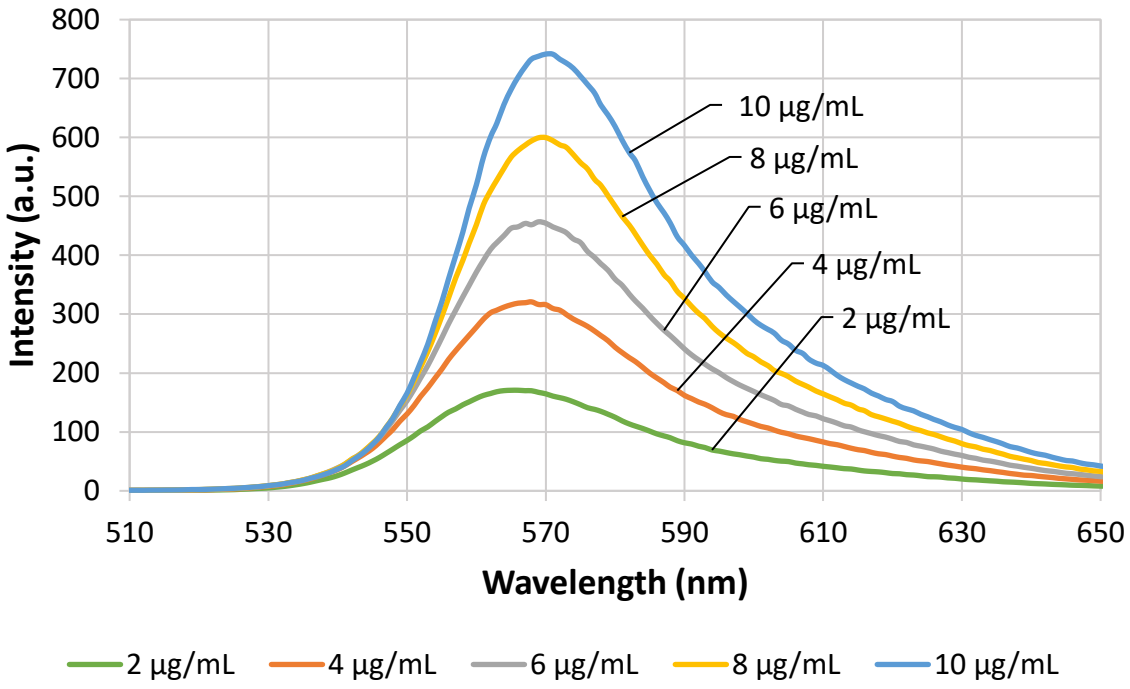

Figure 36. Fluorescence spectra of R6G in DMSO at medium voltage.

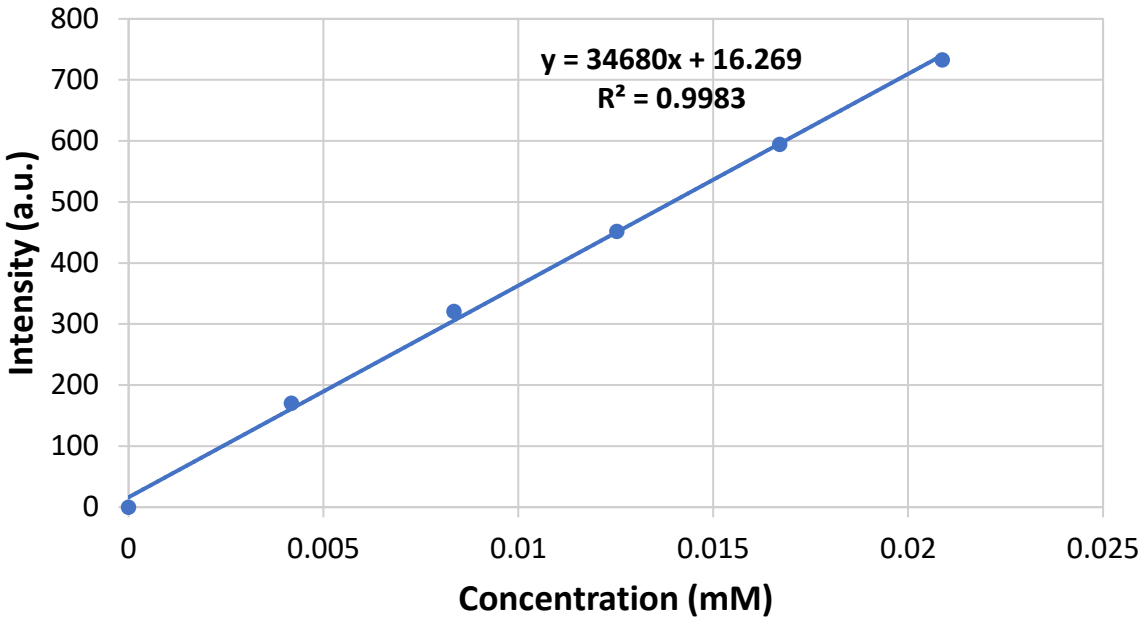

Figure 37. Calibration curve of R6G in DMSO at medium voltage at 568 nm.

The same exact procedure for extraction in DMSO was used for R6G as was used for curcumin. The only difference here was that the concentrations were based on fluorescence intensity rather than UV/Vis absorbance. The encapsulation efficiency procedure was repeated for each batch of R6G-loaded pSi due to the inconsistencies in loading spoken about previously. Although the targeted loading for R6G in pSi was around 20%, the batch of pSi nanoparticles loaded with R6G resulted in an encapsulation efficiency of 14.57%. This value was used to determine the actual amount of the model dye loaded into the pSi throughout the various release studies.

4.3 Rhodamine Release from Porous Silicon Nanoparticles and Alginate Hydrogels in Water

The first release procedure consisted of releasing R6G from loaded pSi nanoparticles in water. This release procedure was the exact same as explained previously for the curcumin-loaded pSi nanoparticles in water, where a known amount of loaded pSi was weighted out into three

separate 2 mL plastic centrifuge tubes, exactly 1 mL of water was pipetted into each of the three tubes, and then they were placed in a shaking incubator set at 37°C for each time interval. The time intervals chosen for this release experiment were 5, 10, 20, 40, and 60 minutes. After each incubation period, the three tubes were removed from the incubator, centrifuged for 2 minutes at 5000 rpm, and the fluorescence intensity of a known volume of the supernatant was measured. After this measurement, the rest of the supernatant was removed from each tube, and a fresh 1 mL of water was pipetted in for the next time interval. The average cumulative percent release of R6G from pSi nanoparticles in water over 1 hour is shown below in **Figure 38**. After the first 5 minutes, an average of 91.71% of the R6G loaded in these pSi nanoparticles was released, and an average of 98.40% was released after 60 minutes.

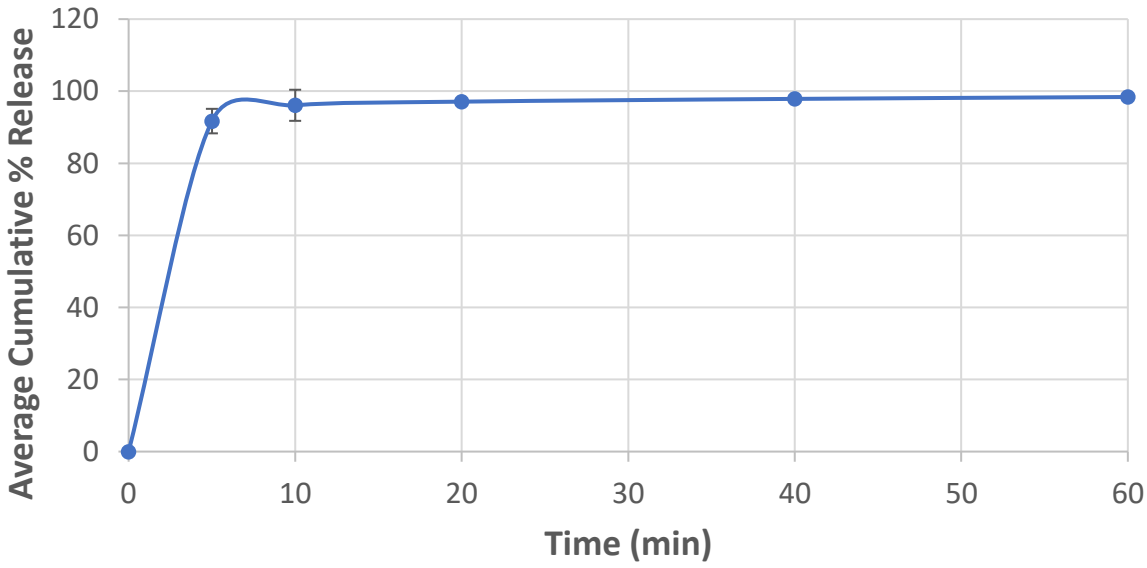

Figure 38. Average cumulative release of R6G from pSi nanoparticles in water.

The second release procedure consisted of releasing R6G from only alginate hydrogels. These hydrogels were constructed the same way as previously described in the methods above, but a known mass of R6G was dissolved into the alginate reagent prior to pipetting it into the molds.

After these hydrogels containing R6G were allowed to gel for a week in the humidity box, they were removed, completely dehydrated, and then placed in 15 mL plastic centrifuge tubes for the release procedure. Using the same time intervals up to 1 hour, the amount of R6G released was measured using the fluorescence spectrophotometer. In this procedure, 5 mL of water were pipetted into the 15 mL centrifuge tubes for each time interval. After each incubation period, the samples were centrifuged in the Cole Parmer Centrifuge to ensure no parts of the alginate hydrogel ended up in the cuvette with the supernatant when measuring the fluorescence intensity. Images of each trial after centrifugation are shown below in **Figure 39**, which demonstrates the degradation of the alginate hydrogel over time as the R6G is released.

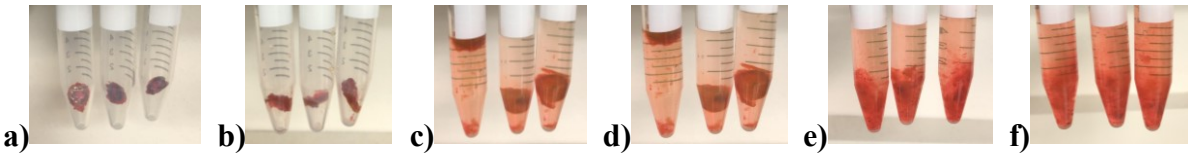

Figure 39. Alginate hydrogels containing R6G during release in water; **a)** initial dehydrated gels, **b)** after 5 min, **c)** after 10 min, **d)** after 20 min, **e)** after 40 min, **f)** after 60 min.

The average cumulative percent release of R6G from alginate hydrogels in water over 1 hour is shown below in **Figure 40.** After the first 5 minutes, an average of 5.73% of the R6G loaded into the alginate hydrogels was released. By 60 minutes, an average of 15.05% of the R6G was released from the alginate hydrogels.

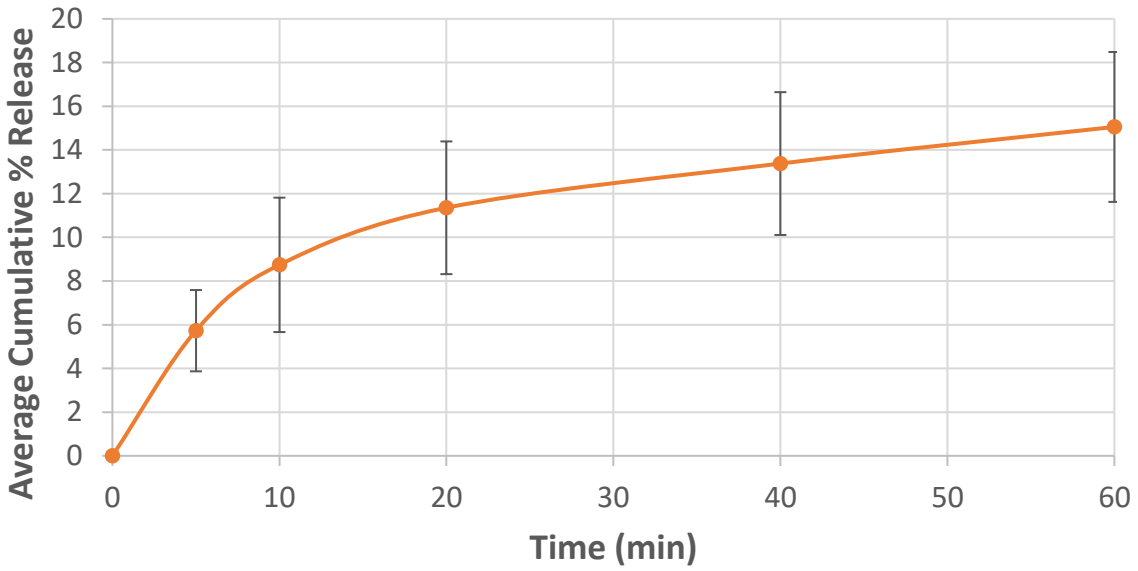

Figure 40. Average cumulative release of R6G from alginate hydrogels in water.

The third release procedure included releasing R6G from pSi that was physically entrapped in alginate hydrogels, which served as the model for the two-system drug delivery mechanism that was desired to be assessed for applications in tissue engineering. The same procedure for releasing R6G from alginate hydrogels only described above was repeated, but this time the hydrogels used in experimentation were the ones created using the "quick aqueous" method as described above, where the R6G-loaded pSi nanoparticles were combined with the alginate prior to gelation of the hydrogels. **Figure 41** below depicts the alginate hydrogels that contained R6G-loaded pSi nanoparticles over a 1-hour period.

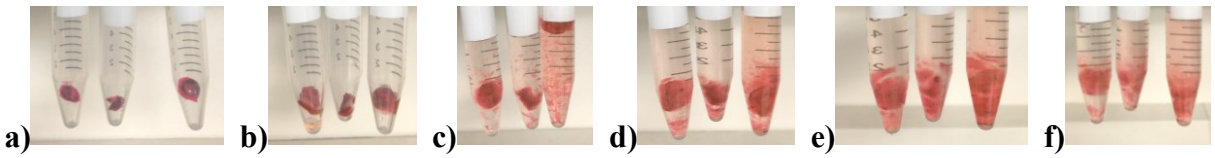

Figure 41. Alginate hydrogels containing R6G-loaded pSi nanoparticles during release in water; **a)** initial dehydrated gels, **b)** after 5 min, **c)** after 10 min, **d)** after 20 min, **e)** after 40 min, **f)** after 60 min.

The average cumulative percent release of R6G from alginate hydrogels in water over 1 hour is shown below in **Figure 42**. After 5 minutes, an average of 4.87% of the R6G loaded into pSi nanoparticles was released from both the pSi and the alginate hydrogel. By 60 minutes, an average of 17.06% of the R6G loaded into the pSi nanoparticles was released from both the pSi and the alginate hydrogel.

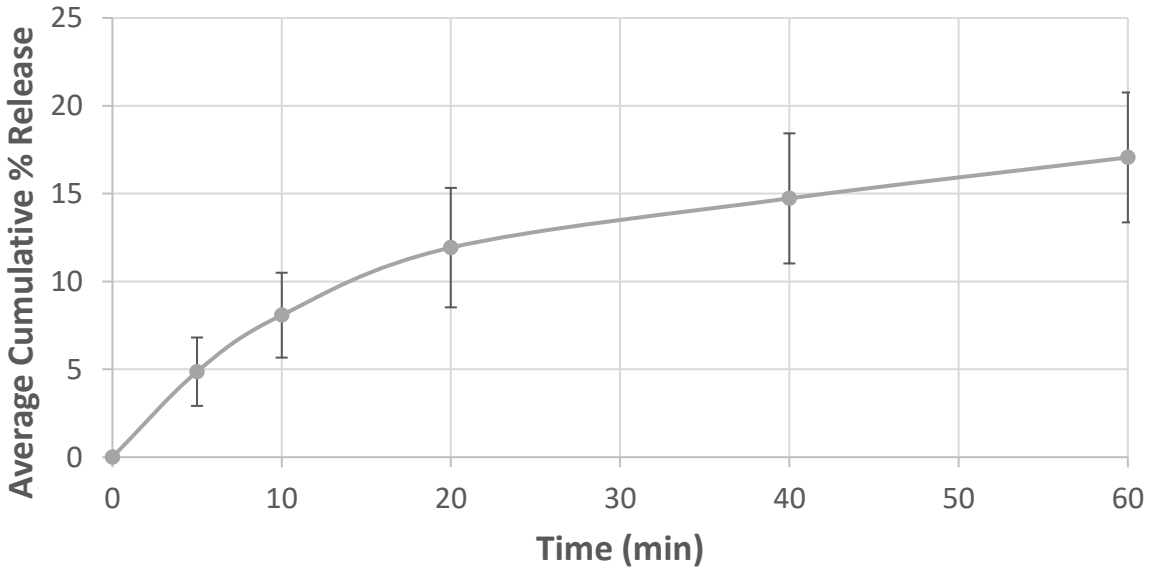

Figure 42. Average cumulative release of R6G-loaded pSi nanoparticles physically entrapped in alginate hydrogels in water.

By overlaying the release profiles of these three separate experiments releasing R6G in water—from pSi nanoparticles only, from alginate hydrogels only, and from pSi nanoparticles physically entrapped in alginate hydrogels—some important takeaways can be seen (**Figure 43**). First, there is a prevalent burst release of the model dye from the pSi nanoparticles, which is

indicated by the 91.71% average cumulative release within the first 5 minutes, which is not an ideal release profile in the context of drug delivery. Furthermore, it can be seen in **Figure 43** that there is barely any difference between the release of the model dye from alginate hydrogels only, or pSi nanoparticles physically entrapped in alginate hydrogels.

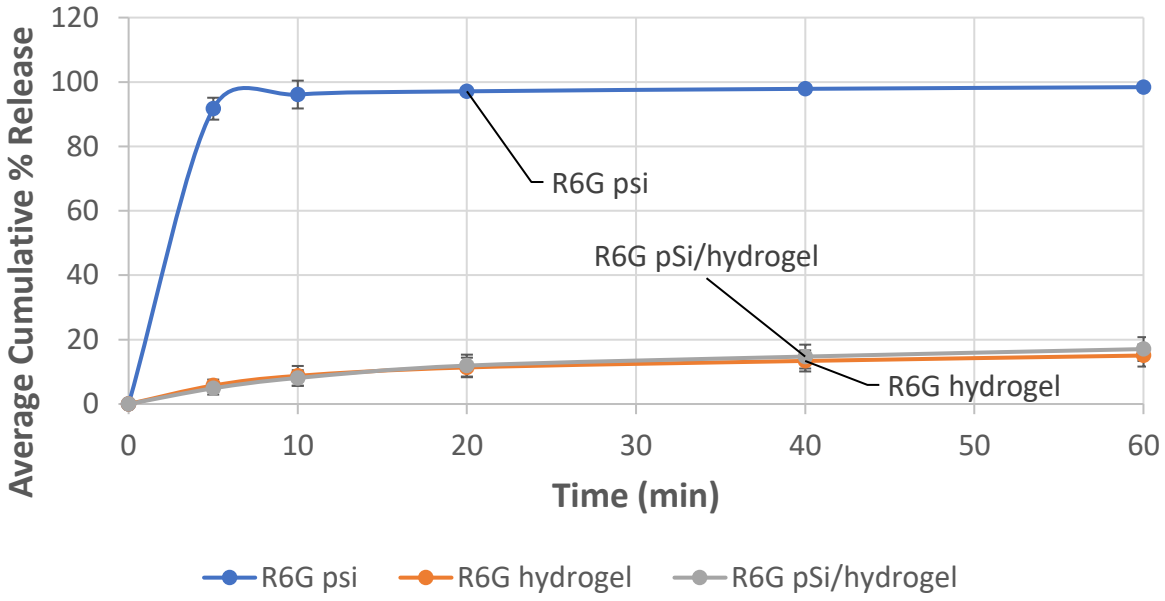

Figure 43. Comparison of R6G release in water from pSi nanoparticles only, alginate hydrogels only, and pSi nanoparticles physically entrapped in alginate hydrogels.

4.4 Rhodamine Release from Porous Silicon Membranes and Alginate Hydrogels

Because R6G was found to release very quickly from pSi nanoparticles, it was decided to measure the release of this same model dye from pSi membranes. Since pSi membranes have a lower internal surface area than pSi nanoparticles, it was thought that physically entrapping pSi membranes into alginate hydrogels would slow down the release of this model dye and exhibit a more ideal release profile for applications in tissue engineering.

Once the pSi membranes were loaded with R6G and placed into alginate hydrogels through the "pSi membrane" method of physical entrapment described above, the hydrogels were allowed to completely dehydrate before being placed in 15 mL centrifuge tubes with 5 mL of water to begin the release experiments. The same procedure for releasing the model dye from these pSi membrane-containing hydrogels as described above was repeated. In this release procedure, the two loading methods of pSi membranes were compared. The first experiment consisted of releasing three trials of alginate hydrogels containing R6G box-loaded pSi membranes for up to three hours (**Figure 44**), and the second experiment consisted of releasing three trials of alginate hydrogels containing R6G tube-loaded pSi membranes for up to three hours (**Figure 45**).

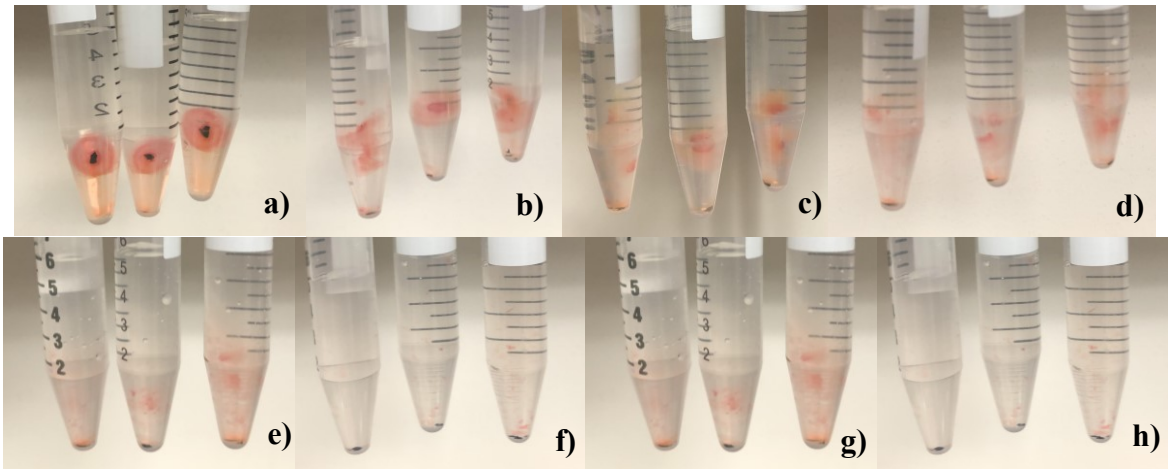

Figure 44. Alginate hydrogels containing R6G box-loaded pSi membranes during release in water; **a)** initial dehydrated gels, **b)** after 5 min, **c)** after 10 min, **d)** after 20 min, **e)** after 40 min, **f)** after 60 min**, g)** after 120 min, **h)** after 180 min.

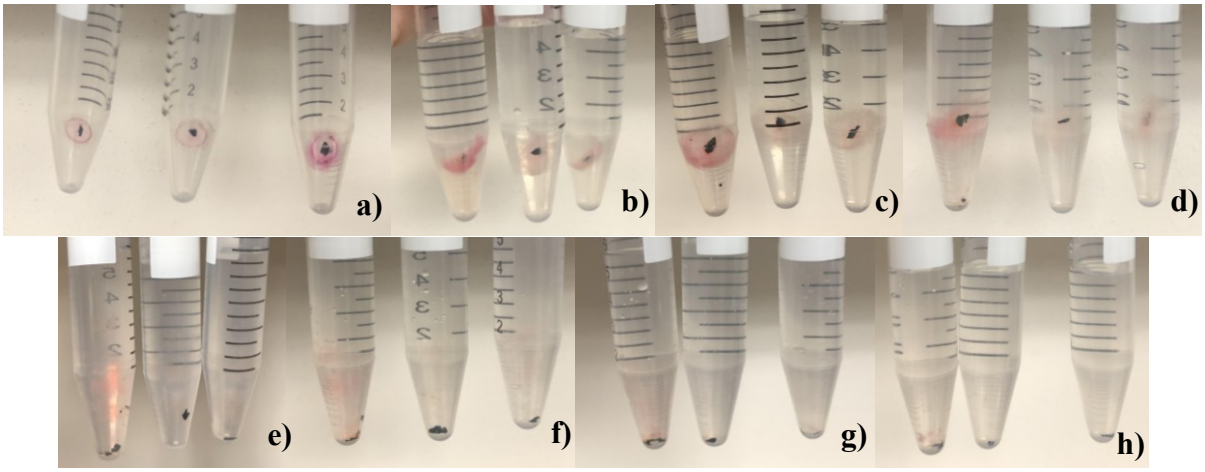

Figure 45. Alginate hydrogels containing R6G tube-loaded pSi membranes during release in water; **a)** initial dehydrated gels, **b)** after 5 min, **c)** after 10 min, **d)** after 20 min, **e)** after 40 min, **f)** after 60 min, **g)** after 120 min, **h)** after 180 min.

The average cumulative percent release of R6G in water from box and tube-loaded pSi membranes physically entrapped in alginate hydrogels is shown below in **Figure 46**. After 1 hour, 4.4% of R6G released from the box-loaded membranes and hydrogels, and 3.9% of R6G released from the tube-loaded membranes and hydrogels. By the third hour of the release experiment, 5.6% of R6G released from the box-loaded membranes and hydrogels, and 5.3% of R6G released from the tube-loaded membranes and hydrogels.

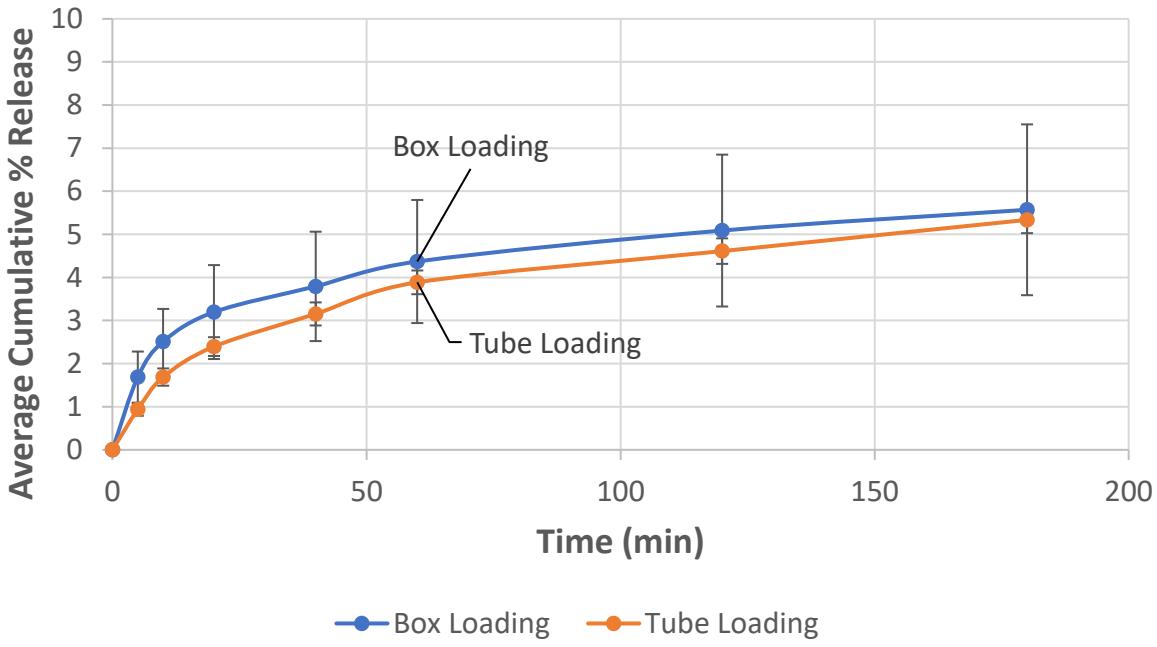

Figure 46. Average cumulative release of R6G box and tube loaded pSi membranes physically entrapped in alginate hydrogels.

Overall, although localization of pSi in alginate hydrogels was achieved through physically entrapping R6G-loaded pSi membranes instead of nanoparticles, the loading of R6G in pSi membranes was not observed to result in high payloads of the model dye when released in an aqueous environment.

Chapter 5. Conclusions and Future Work

In conclusion, this project achieved the overall goal of physically entrapping pSi into alginate hydrogels and monitoring the release of a model dyes from this two-component drug delivery system, which has future applications in the field of tissue engineering. It was first found that curcumin was too hydrophobic of a dye to result in sufficient loading of pSi nanoparticles, as demonstrated by the release profile in an aqueous environment. Therefore, R6G was chosen as the model dye to be loaded and released from both pSi and alginate hydrogels.

Next, physically entrapping pSi nanoparticles in alginate hydrogels was shown to prevent the burst release of the R6G that was observed when releasing from pSi nanoparticles only. Furthermore, localization of pSi in alginate hydrogels was achieved through physically entrapping R6G-loaded pSi membranes into alginate hydrogels. However, the loading of R6G in pSi membranes resulted in low payloads of the dye when released in an aqueous environment. Although it is possible for some highly active therapeutics to benefit from this lower payload in release, a majority of therapeutic drugs require a higher concentration within the body in order to be effective.

In the future, it would be beneficial to choose a specific molecule to optimize the loading of for this model system. Since the magnitude of loading pSi depends on various factors, the molecule chosen ideally would be a dye that has similar structure and properties to a growth factor or therapeutic drug. Once this procedure becomes reliable and repeatable, the release of a therapeutic drug or growth factor from pSi membranes physically entrapped in alginate hydrogels needs to be monitored for potential use in tissue engineering applications.

References

1. O'Brien, Fergal J. Biomaterials & scaffolds for tissue engineering. *Materials Today* **2011**. *14*(3). 88-95.
2. Nataraj, D.; Reddy, N. Chemical Modifications of Alginate and its Derivatives. *International Journal of Chemistry Research*. **2020**. *4*(1). 1-13.
3. Salonen, Jarno. Drug Delivery with Porous Silicon. *Springer International Publishing* **2018**. 3-9.
4. Asadian, M.; Chan; Norouzi; Grande; Silvia; Cools, P.; Morent; Geyter, D. Fabrication and Plasma Modification of Nanofibrous Tissue Engineering Scaffolds. *Nanomaterials*. **2020**. *10*, 119.
5. Sahoo, D.R.; Biswal, T. Alginate and its application to tissue engineering. *SN Applied Sciences*. **2021** *3*(30). doi.org/10.1007/s42452-020-04096-w.
6. Lee, K.Y.; Mooney, D.J. Alginate: Properties and biomedical applications. *Progress in Polymer Science*. **2012**. *37*, 100-126.
7. Feng, Y.; Kopplin, G.; Sato, K.; Draget, K.I.; Varum, K.M. Alginate gels with a combination of calcium and chitosan oligomer mixtures as crosslinkers. *Carbohydrate Polymers*. **2017**. *156*, 490-497.
8. Rescignano, N.; Hernandez, R.; Lopez, L.D.; Calvillo, I.; Kenny, J.M.; Mijangos. Carmen Polymer International. **2016**. *65*(8), 921-926.
9. Shaari, N.; Kamarudin, S.K. Recent advances in additive-enhanced polymer electrolyte membranes properties in fuel cell applications: An overview. *Int J Energy Res.* **2019**. 1-39.
10. Kuo, C.K.; Ma, P.X. Ionically crosslinked alginate hydrogels as scaffolds for tissue engineering: Part 1. Structure, gelation rate and mechanical properties. *Biomaterials*. **2011**. *22*, 511-521
11. Foraker A.B.; Walczak R.J.; Cohen M.H.; Boiarski T.A.; Grove C.F.; Swaan P.W. Microfabricated porous silicon particles enhance paracellular delivery of insulin across intestinal Caco-2 cell monolayers. Pharm Res. **2003**. *20*(1), 110–116.
12. Cam M.E.; Yildiz S.; Alenezi H.; Cesur S.; Ozcan G.S.; Erdemir G.; Edirisinghe U.; Akakin D.; Kuruca D.S.; Kabasakal L.; Gunduz O.; Edirisinghe, M. Evaluation of burst release and sustained release of pioglitazone-loaded fibrous mats on diabetic wound healing: an in vitro and in vivo comparison study. *J. R. Soc. Interface.* **2020**. *17*. 1-3.
13. Santini J.T. Jr; Richards A.C.; Scheidt R.; Cima M.J.; Langer R. Microchips as Controlled Drug-Delivery Devices. *Angew Chem Int Ed Engl.* **2000**. *39*(14), 2396-2407.

14. Canham, Leigh. Routes of Formation for Porous Silicon. *Springer International Publishing*. **2018**. 387-388.

15. Canham, Leigh. Handbook of Porous Silicon. *Springer International Publishing*. **2014**. 3-9.

16. Sailor, Michael J. Porous Silicon Nanoparticles. *Springer International Publishing*. **2018**. 3-9.

17. Entwistle, J.; Reenie, A.; Patwardhan, S. A review of magnesiothermic reduction of silica to porous silicon for lithium-ion battery applications and beyond. *J. Mater. Chem. A.* **2018**. *6*, 18344.

18. Salonen J.; Laitinene L.; Kaukonen A.M.; Tuura J.; Bjorkqvist M.; Heikkila T.; Vaha-Heikkila K.; Hirvonen J.; Leho V.P. Mesoporous silicon microparticles for oral drug delivery: loading and release of five model drugs. *J Control Release*. **2005**. *108*. 362-374.

19. Ganguly, R.; Kumar, S.; Kunwar, A.; Nath, S.; Sarma, H.D.; Tripathi, A.; Verma, G.; Chaudhari, D.P.; Aswal, V.K.; Melo, J.S. Structural and therapeutic properties of curcumin solubilized pluronic F127 micellar solutions and hydrogels. *Journal of Molecular Liquids*. **2020**. *314*. 1-7.

20. Anand, P.; Kunnumakkara, A.B.; Newman, R.A.; Aggarwal, B.B. Bioavailability of Curcumin: Problems and Promises. *Molecular Pharmaceutics*. **2007**. *6*(6), 807-818

21. Banerjee, C.; Maiti, S.; Mustafi, M.; Kuchlyan, J.; Banik, D.; Kundu, N.; Dhara, D.; Sarkar, N. Effect of Encapsulation of Curcumin in Polymeric Nanoparticles: How Efficient to Control ESIPT Process? *Langmuir*. **2014**. *30*, 10834-10844.

22. Al-Kadhemy, M.F.; Alsharuee, I.F.; Al-Zuky, A.; Ali A.D. Analysis of the Effect of the Concentration of Rhodamine B in Ethanol on the Fluorescence Spectrum using the "Gauss Mod" Function. *Journal of Physical Science*. **2011**. *22*(2), 77-86.

23. Bakkialakshmi, S.; Selvarani, P.; Chenthamarai, S. Fluorescnece quenching of Rhodamine B base by two amines. *Spectrrochimica Acta Part A: Molecular and Biomolecular Speectroscropy.* **2013**. *105*, 557-562.

24. Gorwney K.; Emily A.; Flores, R.; Bledsoe, G.J.; Sell, S.A. Characterization of slow-gelling alginate hydrogels for intervertebral disc tissue-engineering applications. *Materials Science and Engineering.* **2016**. *63*, 198-210.

25. Zhang, Zhiping; Feng, Si-Shen. The drug encapsulation efficiency, in vitro drug release, cellular uptake and cytotoxicity of paclitaxel-loaded poly0lactide)-tocopheryl polyethylene glycol succinate nanoparticles. *Biomaterials*. **2006**. *27*, 4025-4033.